BIOCHEMISTRY
including biophysical chemistry & molecular biology

Article

pubs.acs.org/biochemistry

Extensive Simulations of the Full-Length Matrix Metalloproteinase-2 Enzyme in a Prereactive Complex with a Collagen Triple-Helical Peptide

Natalia Díaz* and Dimas Suárez

Departamento de Química Física y Analítica, Universidad de Oviedo, Julián Clavería 8, Oviedo, Asturias, 33006 Spain

Supporting Information

ABSTRACT: Collagen hydrolysis catalyzed by matrix metalloproteinases is an important and complex process involved in a variety of physiological and pathological conditions. To contribute to its characterization at the molecular level, herein we analyze three different models for the complex formed between the full-length matrix metalloproteinase-2 (MMP-2) enzyme and a synthetic triple-helical peptide (fTHP-5). The considered MMP-2/fTHP-5 complexes mainly differ in the location of the C-terminal hemopexin-like domain, but in all of them, the middle α-chain of the substrate (B-chain) is placed within the active site groove. We performed extended molecular dynamics (MD) simulations to determine the most likely rearrangements of the MMP-2 domains in response to the presence of the triple helix. The relative stability of the MD models is assessed in terms of molecular mechanics Poisson−Boltzmann calculations and approximate estimations of configurational entropy. In addition, the most significant MMP-2···fTHP-5 interactions at the catalytic and noncatalytic domains are also analyzed to gather some clues about the role of the different domains during collagenolysis.

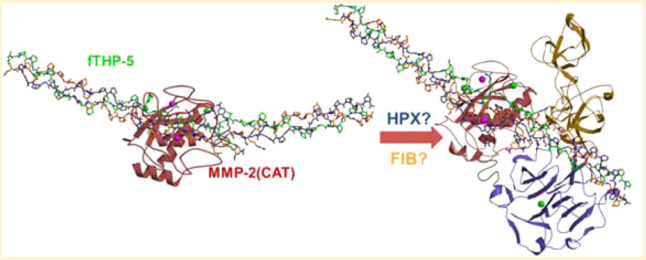

Matrix metalloproteinases (MMPs) are zinc- and calcium-dependent endopeptidases that operate in the extracellular environment by proteolytically processing a wide range of extracellular and intracellular proteins.[1,2] The substrates of the MMPs are not limited to matrix proteins; cytokines, growth factors, cell adhesion proteins, and receptors are also included. As a result, the MMPs are currently considered as multifunctional enzymes that play crucial roles in a number of physiological and pathological conditions.[3] For instance, MMP-2 is a ubiquitous protein involved in the remodeling of the extracellular matrix, a function that is associated with the hydrolysis of protein substrates like collagen and fibronectin. It also plays a beneficial anti-inflammatory role because of its action over a number of chemokines, but it has been validated as an anticancer drug target because of its relevance during tumor growth, angiogenesis, and metastasis.[2,4]

The MMPs are multidomain enzymes composed of a catalytic (CAT) domain and other modules or domains that seem to provide substrate specificity or guide their cellular location.[5] The CAT domain (~165 residues) displays a similar structure in all the enzymes, with three α-helices, a five-stranded twisted β-sheet, and several surface loops.[6] The active site is a narrow cleft that is delimited by the fourth strand of the β-sheet, the last portion of the so-called S-loop that connects strands β3 and β4, and the specificity or Ω-loop.[7] Peptide substrates extend along this active site by establishing a number of polar and hydrophobic interactions, whereas the scissile peptide bond is placed in the middle of the cleft close to the catalytic zinc ion.[8,9] Additionally, CAT binds a second zinc and several calcium ions, which contribute to the stabilization of the configuration of several loops.[10]

In most MMPs, the noncatalytic domains include a hemopexin-like (HPX) domain joined to CAT by a linker of variable length.[6] The polypeptide chain in HPX (~200 residues) is essentially organized in four β-sheets (blades I−IV) and arranged almost symmetrically around a central channel giving rise to a four-blade propeller.[11] With regard to its function, HPX is involved in the activation and inhibition of several MMPs. It also contributes to the localization of the MMPs at the cellular surface because of its binding to other cell-bound proteins.[12] Experimental results also suggest that HPX may play a critical role during the binding and cleavage of protein substrates like fibrillar collagen.[13−16]

Collagen is a remarkable substrate of the MMPs that is characterized by a large triple-helical structure. To improve our understanding of the stability of this triple helix and its interaction with other proteins, synthetic triple-helical peptides (THPs) have been developed as reduced collagen models.[17] Molecular docking efforts to place a THP on the crystal structure of MMP-1 resulted in severe steric clashes,[18] suggesting that the intact triple helix does not fit into the active site of the enzyme and that the triple helix has to locally unwind prior to its hydrolysis, a process that is commonly

Received: August 13, 2014
Revised: December 15, 2014
Published: January 20, 2015

DOI: 10.1021/bi501014w
Biochemistry 2015, 54, 1243−1258

Scheme 1

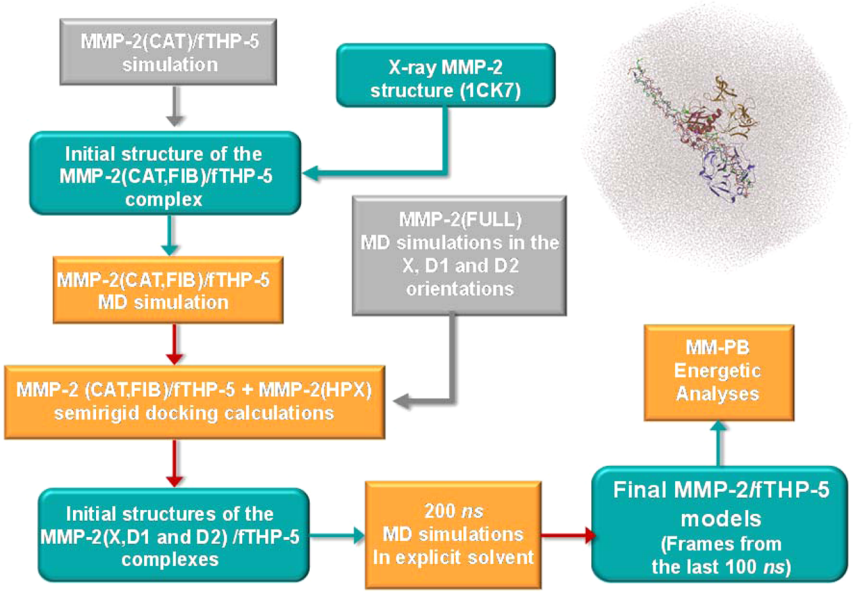

thought to be facilitated by the interplay between CAT and other MMP domains like HPX.

Secondary sites for collagen/THP binding located outside the active site, and termed exosites, have been found on the HPX domain of MMP-1.[5] Hydrogen/deuterium exchange mass spectrometry shows that a C-terminal extended THP exhibits protection to exchange in three regions (residues 287−295, 304−316, and 439−457) of the MMP-1 HPX domain.[19] The region of residues 287−295 is located in the first strand of blade I, and according to molecular modeling analysis, it is the most proximal to the triple helix. Mutagenesis and kinetic experiments have also been performed to confirm that Ile_{290} and Arg_{291} participate in the binding and catalysis of the triple helix. In another hydrogen/deuterium exchange mass spectrometry study, three MMP-1 regions located in HPX [residues 266−277, 283−297, and 330−346 in the structure of Protein Data Bank (PDB) entry 4AUO] have also shown delayed deuterium incorporation in the presence of collagen I.[20] In this case, docking analysis and mutagenesis experiments performed for selected residues suggest that residues Ile_{271}, Arg_{272}, and Phe_{301} constitute the so-called hydrophobic $S_{10'}$ exosite in the HPX domain, which binds the 10th residue C-terminal to the scissile peptide bond. This work also presents what is perhaps the most defined view to date of the interaction of a THP with MMP-1: an X-ray structure revealing polar and hydrophobic contacts between the THP and the HPX domain involving, among others, residues Ile_{271}, Met_{276}, Phe_{301}, and Trp_{302} and the alkyl portion of Arg_{272} for binding Leu($P_{10'}$) and residues Val_{300} and Phe_{301} for Ile($P_{7'}$). Unfortunately, this crystallographic structure corresponds to an unproductive complex because the scissile Gly(P_1)−Leu($P_{1'}$) peptide bond is not placed within the active site cleft.

Very recently, nuclear magnetic resonance (NMR) measurements have mapped the interaction between the HPX domain of MMP-1 and a THP model of collagen I to residues Arg_{291}, Gly_{292}, Glu_{311}, Glu_{313}, Asn_{315}, Phe_{316}, Ile_{317}, Ser_{318}, Val_{319}, Phe_{320}, Gln_{323}, and Asn_{326} in the HPX domain.[21] On the basis of these NMR results, docking analyses have been used to generate a set of MMP-1/THP complexes supposed to be relevant for the initial binding, unwinding, and hydrolysis of the triple helix. On the basis of these models, a collagenolysis mechanism that requires a rearrangement of the CAT and HPX relative position has been proposed to allow the binding of the scissile peptide bond within the MMP-1 active site. In fact, this relative movement of CAT and HPX had been previously considered to provide the driving force for collagen distortion and triple helicase activity.[5] Experimental evidence supporting such intramolecular flexibility between CAT and HPX has been obtained for different MMPs, either alone or in complex with collagen.[22−26] In addition, molecular simulations performed for full-length MMP-2 indicate that alternative configurations with respect to that observed in the X-ray structure could be energetically accessible to the enzyme in an aqueous solution.[27,28]

Gelatinases (MMP-2 and MMP-9) also hydrolyze the triple helix of different collagen types.[29] They possess an additional domain inserted into the primary sequence of CAT that is formed by three individual consecutive repeats with homology to the gelatin binding (type II) domain of fibronectin.[6] This fibronectin-like (FIB) domain is involved in the binding of denatured forms of collagen (gelatin), and it has been termed by several authors the collagen binding domain (CBD).[30,31] Each FIB module (FIB1−FIB3) possesses a binding site formed by conserved aromatic residues (Phe_{256}, Trp_{258}, Phe_{265}, Tyr_{271}, and Phe_{273} in FIB1; Phe_{297}, Try_{314}, Trp_{316}, Tyr_{323}, Tyr_{329}, and Phe_{331} in FIB2; Phe_{335}, Trp_{374}, Tyr_{381}, Trp_{387}, and Phe_{389} in FIB3) that are oriented away from each other so they do not form a continuous binding motif.[32−34] However, other authors consider that the collagen binding properties of MMP-2 reside in its HPX domain, whereas the FIB domain is involved in only the processing of gelatin.[15]

In our previous work, we have analyzed the interaction of the isolated CAT domain of MMP-2 with a synthetic triple-helical peptide (fTHP-5) mimicking the amino acid sequence of collagen type II around the scissile peptide bond recognized by the MMPs {[aC_6-(Gly-Pro-Hyp)$_5$-Gly_{17}-Pro_{18}-LAmp$_{19}$-Gly_{20}-Pro_{21}-Gln_{22}-Gly_{23}-Leu_{24}-Arg_{25}-Gly_{26}-Gln_{27}-Dnp$_{28}$-Gly_{29}-Val_{30}-Arg_{31}-(Gly-Pro-Hyp)$_5$-NH_2]$_3$}.[35] Previous results showed that fTHP-5 is efficiently hydrolyzed by the MMP-2 enzyme at the Gly_{23}−Leu_{24} and Gly_{26}−Gln_{27} bonds.[36] By means of potential

DOI: 10.1021/bi501014w
Biochemistry 2015, 54, 1243−1258

mean force calculations used to distort locally the Gly_{23}−Leu_{24} linkages, followed by docking analyses and molecular dynamics (MD) simulations, we built different MMP-2(CAT)/ fTHP-5 complexes in which each of the three α-chains of the triple helix (A, B, or C) is placed within the MMP-2 active site in a prereactive configuration. The computational models have confirmed that the CAT domain selects chain B (the central chain) as the one to be hydrolyzed in the first place. In addition, the models show that the MMP-2 catalytic domain is not significantly distorted in the prereactive complexes, but the central region of the fTHP-5 triple helix is completely unwound and occupies the MMP-2 active site groove. Thus, the CAT··· fTHP-5 interactions can be seen to be crucial to maintaining an unwound triple helix prior to its hydrolysis.

In this work, we take one additional step and investigate the structure of prereactive complexes between the full-length MMP-2 enzyme and fTHP-5. Starting with the best MMP-2(CAT)/fTHP-5(B) model, we first incorporate the FIB domain in the orientation observed for the full-length pro-MMP-2 and the resulting structure is relaxed by performing an MD simulation in explicit solvent. Second, the HPX and linker domains are added to assemble the full-length enzyme. Three different relative orientations of the HPX domain with respect to CAT are considered: the one observed in the X-ray structure of the pro-MMP-2 enzyme[37] and two other plausible orientations obtained in our previous study.[28] In this way, we obtain three models for the full-length MMP-2 enzyme bound to the distorted fTHP-5 substrate that are relaxed by extensive MD simulations (200 ns). The relative stability of the three configurations is assessed by means of molecular mechanics Poisson−Boltzmann (MM-PB) calculations and approximate configurational entropy calculations. Overall, the analyses of the trajectories allow us to identify the interaction sites with the noncatalytic domains and to evaluate if they could contribute to the further perturbation of the structure of the triple helix at the prereactive complex.

METHODS

The structural elements and the methodological workflow that have been used to construct the dynamical models of the prereactive complex between the full-length MMP-2 enzyme and the fTHP-5 system are summarized in Scheme 1 and described in detail below.

MM Parameters. We employed the same set of MM parameters that were used in our previous simulations of the native form of full-length MMP-2 and the MMP-2(CAT)/ fTHP-5 complexes.[28,35] Thus, the parm03 version of the all-atom AMBER force field (AMBER03) was used to model the systems,[38] and the TIP3P potential[39] was used for water molecules. For the nonstandard residues included in the fTHP-5 ligand (Ac_6, Hyp, LAmp, Dnp, and NH_2), we employed the set of parameters compatible with AMBER03 that has been described elsewhere.[35] For the zinc and calcium ions, we used a set of AMBER03-like parameters that have been derived and validated by us in previous works.[10,40,41] In particular, for the catalytic Zn_1, we followed a mixed bonded and nonbonded approach in which the metal ion is linked to the Nε atoms of the His_{403}, His_{407}, and His_{413} ligands and the bridging water molecule {i.e., $[Zn\text{-}(OH_2)]^{2+}\cdots{}^{-}OOC\text{-}Glu_{404}$} by explicit MM bonds while the fifth (apical) position of the Zn_1 ion is represented by nonbonded parameters. The reference bond lengths and angles for the Zn_1 coordination sphere were obtained from quantum mechanical/molecular mechanics (QM/MM) energy minimizations of the MMP-2 catalytic domain.[10] The corresponding force constants were estimated numerically by means of QM gradient calculations on cluster models extracted from the QM/MM structures. Similarly, the atomic charges for the Zn ion and its ligands were fit to reproduce the QM electrostatic potential of the cluster models using the RESP methodology[42] and QM methods prescribed in the AMBER03 force field.[38] The van der Waals ε parameter for Zn_1 is assigned an intermediate value between those of the bonded and nonbonded representations, and the Zn_1 apical water molecule is assigned the TIP3P charges during the RESP fitting procedure.[10] In this way, the same set of parameters for the Zn_1 site has been used to conduct MD simulations of the unbound and bound states of the MMP-2 enzyme, the Zn_1 apical position being occupied by TIP3P water molecules and the carbonyl group of peptide substrates, respectively.[9,41] Overall, the parametrization of the nonstandard residues in fTHP-5 and the Zn_1/Zn_2 coordination environments ensures that the bonded and nonbonded interactions among all atoms of the enzymatic system are treated on an equal basis, thereby minimizing potential MM artifacts.

Setup of the MMP2(CAT-FIB)/fTHP-5 Model. Initial coordinates for the different MMP-2/fTHP-5 models considered in this work were obtained from previous simulations and from the crystal structure of PDB entry 1CK7 of the full-length pro-MMP-2 enzyme. In particular, the coordinates of MMP-2(CAT) and fTHP-5 fragments were taken from the MD snapshot after 50 ns of the MMP-2(CAT)/fTHP-5(B) simulation.[35] The three FIB modules were initially modeled as arranged in the 1CK7 crystal structure.[37] In this experimental structure, the relative orientation of FIB with respect to CAT seems to be determined by the presence of the pro-peptide (Pro_{31}−Asn_{109}), which simultaneously places the cysteine-switch strand (Pro_{100}-Arg_{101}-Cys_{102}-Gly_{103}) coordinated to the catalytic Zn ion and the Phe_{37} side chain within the FIB3 hydrophobic pocket. We reasoned that this relative position of CAT and FIB would be a favorable orientation to allow the fTHP-5 molecule to interact with the two domains in a hypothetical MMP-2(CAT-FIB)/fTHP5 complex. Thus, we superposed several backbone coordinates of CAT in the 1CK7 crystal structure onto the corresponding ones in the selected MMP-2(CAT)/fTHP-5(B) snapshot, and the coordinates of FIB in the superposed 1CK7 structure were finally added to replace the Gly_{216}-Lys-Gly-Val-Gly_{394} connection loop (1CK7 numbering) in the MMP-2(CAT)/fTHP-5(B) snapshot. The resulting **MMP-2(CAT-FIB)/fTHP5** complex was relaxed by means of an 85 ns MD simulation in explicit solvent following the computational prescriptions that are described below.

Building the Initial Structures for the MMP2(FULL)/fTHP-5 Models by Docking the HPX and Linker Domains within MMP2(CAT-FIB)/fTHP-5. The initial structures of the MMP2(FULL)/fTHP-5 complexes were built by means of a semirigid docking protocol that combines a set of MD structures for the **MMP-2(CAT-FIB)/fTHP-5** complex with another set of MD structures for the active full-length MMP-2.[28] The docking process, which is very similar to that employed in previous works for the construction of the full-length MMP-2 models[27,28] and the MMP-2(CAT)/fTHP-5 complexes,[35] consisted of the following steps.

(1) We selected 50 equally spaced structures from the last 80 ns of the **MMP-2(CAT-FIB)/fTHP-5** MD simulation. Each structure contained both the coordinates of the solute atoms and a 3.0 Å layer of water molecules around the solute.

DOI: 10.1021/bi501014w
Biochemistry 2015, 54, 1243−1258

However, coordinates of the protein atoms and the water molecules were saved separately, because only the protein atoms were considered in the docking calculations.

(2) On the basis of the results of our previous study of the active full-length MMP-2,[28] we retrieved 50 snapshots of the solute atoms (and a 3.0 Å layer of water molecules that were again saved separately) from each of the three 200 ns MD trajectories that differ in the orientation of the HPX domain and are labeled as **X**, **D-1**, and **D-2**.

(3) Each of the MMP-2(FULL) structures was docked onto the **MMP2(CAT-FIB)/fTHP-5** snapshots by superposing the backbone atoms of the secondary structure elements of the CAT domain and then removing the CAT-FIB atoms from the full-length structure. Only the solute protein atoms of the ligand/host systems were considered at this stage. Three different sets of MMP-2/fTHP-5 complexes [i.e., **MMP-2(X)/fTHP-5**, **MMP-2(D-1)/fTHP-5**, and **MMP-2(D-2)/fTHP-5**] depending on the orientation of HPX with respect to CAT-FIB were generated. Each set included 50 × 50 = 2500 structures.

(4) For every single MMP-2(FULL)/fTHP-5 model, steric clashes between the linker and HPX domains and the rest of the system were iteratively identified and locally relaxed. The coordinates of the clashing residues were optimized by conducting 1000 conjugate gradient steps followed by 25 ps of MD using the AMBER03 force field and a distance-dependent dielectric constant ($\varepsilon = 4r_{ij}$). A high temperature value (500 K) was used in the restricted MD simulations to promote uphill moves of bulky side chains that can be important for properly relaxing some steric collapses. Once the loop over all the steric clashes had been completed, the coordinates of the linker region were fully optimized.

(5) To energetically score the partially relaxed models, we estimated the conformational energy of the linker region and the interaction energies between the linker and HPX domains and MMP-2(CAT)/fTHP-5 moieties by performing single-point MM-PB energy calculations on the full MMP-2/fTHP-5 complexes and on the separated fragments.[27] These calculations were conducted using the PBSA program in Amber10[43] with settings similar to those detailed below for the MM-PB analyses of the MD simulations. We observed that all the models that are favorably ranked at this stage are derived from structures that show none or just a few steric clashes between the HPX and linker domains and the CAT/FIB/fTHP-5 residues. More particularly, the most favorable **MMP-2(X)/fTHP-5** and **MMP-2(D-1)/fTHP-5** models exhibited zero clashes while the corresponding **MMP-2(D-2)/fTHP-5** model had only three bad contacts involving the $Asn_{430}\cdots Ala_{607}$, $Arg_{432}\cdots Pro_{614}$, and $Ser_{448}\cdots Asp_{450}$ residue pairs.

(6) The structural quality information about the best MMP-2(FULL)/fTHP-5 models was further analyzed using WHAT_CHECK.[44] Finally, the water molecules from the 3.0 Å solvent layer of the separate MMP-2(FULL) and **MMP-2(CAT-FIB)/fTHP-5** fragments that did not show any steric clash among protein atoms or other water molecules were included in the best models for setting up the corresponding MD simulations. In this way, the first solvation shell of the initial complexes is preadapted to the protein atoms and preserves the location of some structural water molecules.

MD Simulations in Explicit Solvent. The final MMP-2(FULL)/fTHP-5 structures generated by the docking process were surrounded by octahedral periodic boxes of TIP3P water molecules that extended 18 Å from the 3.0 Å water shell. A rectangular box was used instead for the **MMP-2(CAT-FIB)/fTHP-5** model. In addition, four and three Na^+ counterions were placed to neutralize the **MMP-2(CAT-FIB)/fTHP-5** and MMP2(FULL)/fTHP-5 systems, respectively, resulting in a total of 7004 and 10365 protein atoms being solvated by ∼65500 and ∼100000 water molecules, respectively.

Periodic boundary conditions were applied to simulate continuous systems, and long-range interactions were described by the particle mesh Ewald method with a grid spacing of ∼1 Å and a nonbonded cutoff of 10.0 Å. Solvent molecules and Na^+ counterions were initially relaxed by means of energy minimizations and 100 ps of MD at 300 K. Then, the full systems were minimized and heated gradually to 300 K during 120 ps of MD. The production phase of the simulations, which were run at constant pressure (1 bar) and temperature (300 K) with a time step of 2 fs, comprised 85 ns for the **MMP-2(CAT-FIB)/fTHP-5** model and 200 ns for the three MMP-2(FULL)/fTHP-5 models. Coordinates were saved every 2 ps. All the energy minimizations and MD calculations were performed with NAMD version 2.7.[45] Structural analyses were conducted with the *ptraj* program included in the Amber10 package and some other specific software developed locally. Clustering analyses were performed for the fTHP-5 molecule by using the MMTSB ensemble tools and considering the root-mean-square deviations of the backbone Cα atoms and a radius of 3 Å.[46]

QM/MM Calculations. From the **MMP-2(X)/fTHP-5** MD simulation, we selected a representative snapshot to optimize the Zn_1 coordination environment by means of QM/MM calculations. The selected snapshot was truncated by including the MMP-2/fTHP-5 atoms solvated by a water shell with a thickness of 15.0 Å (∼17000 water molecules). The QM/MM geometry optimizations were conducted with the *sander* program included in the Amber12 package,[47] which provides an QM/MM interface with the QM *Gaussian09* package.[48] Hydrogen link atoms were placed by *sander* at the His_{403} Cβ−Cα, His_{407} Cβ−Cα, His_{413} Cβ−Cα, and Glu_{404} Cβ−Cα bonds of MMP-2 and the P_2 C−Cα and $P_{2'}$ N−Cα bonds in chain B of fTHP-5. In addition, the QM region also included the catalytic Zn_1 ion, the Wat1 molecule, which has an explicit Zn_1−O bond in the force field representation, a second water molecule that occupies an axial coordination around Zn_1 as observed during the simulation, and two other water molecules located near the catalytically important Zn_1−Wat···$^-$OOC−Glu_{404} contact. This partitioning resulted in a QM region comprising a total of 97 QM atoms with a net charge of +1 that was described at the B3LYP/6-31+G* level of theory[49,50](989 basis functions). The rest of the protein and solvent atoms were treated with the AMBER03 force field. During the QM/MM geometry optimization, all the protein residues and water molecules that have an atom within a 8.0 Å sphere centered at the Zn_1 ion were allowed to move. The position of the rest of the protein and solvent molecules was frozen. The QM/MM energy minimization was performed with no cutoff until the root-mean-square deviation of the Cartesian elements of the gradient was less than 0.02 kcal mol^{-1} $Å^{-1}$ (2×10^{-5} au).

Electrostatic Calculations. The electrostatic potential of the MMP-2 models in solution was computed on selected snapshots from the MD trajectories using the APBS software.[51] In the PB calculations, atomic charges and radii were taken from the *parm03* representation. The linearized PB equation was solved on a cubic lattice by using an iterative finite-difference method. The cubic lattice had a grid spacing of 0.33 Å, and the points at the boundary of the grid were set to the sum of Debye−Hückel potentials. The dielectric boundary was

DOI: 10.1021/bi501014w
Biochemistry 2015, 54, 1243−1258

the contact surface between the radii of the solute and the radius (1.4 Å) of a water probe molecule. The electrostatic potential was plotted onto the molecular surface computed by the MSMS program using the Chimera visualization system.[52]

Energetic Analyses of the MD Trajectories. To assess the relative stability of the MMP-2(FULL)/fTHP-5 complexes, we employed the MM-PB method.[53,54] This approach, which is normally classified as an end-point free energy method,[55,56] has been intensively used in different variants to calculate the binding energy of protein−ligand complexes[57] such as, for example, those formed between the HIV-1 protease and potent inhibitors.[58] This class of end-point free energy methods can also estimate the binding energy of protein/peptide or protein/protein complexes studied by MD simulations (see, for example, refs 54 and 59−63). Similarly, we have previously assessed, in terms of average MM-PB energies, the alternative configurations of the full-length MMP-2 enzyme in its native form and the various modes of binding between the MMP-2 catalytic domain and fTHP-5.[28,35] The MM-PB energy expression is often considered as a physically based scoring function that provides accurate rankings of nativelike loop configurations[64] and constitutes an appropriate benchmark to evaluate, by comparison, the performance of faster and more empirical scoring functions for protein−protein or protein−ligand docking calculations.[65]

The MM-PB calculations reported in this work were conducted on 2000 snapshots extracted from each MD simulation every 100 ps after having removed all solvent molecules and counterions. For comparative purposes, we also applied the MM-PB protocol on 1000 snapshots extracted from the last 100 ns of our former MD simulations[28] of the full-length MMP-2 enzyme in its unbound form and on 500 snapshots retrieved from the 50 ns MD trajectory[35] of fTHP-5 in its triple-helical state.

The MM-PB energy was computed according to the following equation:[54]

$$G_{\text{MM-PB}} = E_{\text{MM}} + \Delta G_{\text{solv}}^{\text{PB}} + \Delta G_{\text{solv}}^{\text{nonpolar}} \quad (1)$$

where E_{MM} is the molecular mechanics energy including the $3RT$ contribution due to six translational and rotational degrees of freedom, $\Delta G_{\text{solv}}^{\text{PB}}$ is the electrostatic solvation energy obtained from Poisson−Boltzmann calculations,[66] and $\Delta G_{\text{solv}}^{\text{nonpolar}}$ is the nonpolar part of the solvation energy due to cavity formation and van der Waals interactions between the solute and the solvent molecules. A solvent-accessible surface area (SASA)-dependent term is typically employed to calculate the nonpolar solvation energy (i.e., $\Delta G_{\text{solv}}^{\text{nonpolar}} = a \times \text{SASA} + b$). However, the SASA approximation has potential problems because it neglects molecular shape effects and because of the implicit assumption that the contribution of dispersion interactions has the same form of cavity formation costs.[67] Taking into account the fact that these limitations could be more accentuated in the case of protein−protein complexes, we estimated the nonpolar solvation using the following approximation introduced by Gohlke and Case:[54]

$$\Delta G_{\text{solv}}^{\text{nonpolar}} = \Delta H_{\text{solute-solvent}}^{\text{vdW}} + \gamma \text{MSA}$$

where $\Delta H_{\text{solute-solvent}}^{\text{vdW}}$ is the van der Waals (vdW) interaction energy between the solute and the water molecules within a shell with a thickness of 12 Å, while the cavitation free energy contribution to the nonpolar solvation energy is determined by a molecular surface area (MSA)-dependent term. This approach includes the favorable van der Waals dispersion between all the solute atoms and the nearby solvent molecules, which need to be considered when assessing the stability of protein−protein complexes in which the number of solvent-exposed and buried atoms can differ considerably.[54] All the computational details for obtaining the various MM-PB components were identical to those used in our previous study.[28]

The MM-PB energy expression (eq 1) does not take into account the configurational entropy (S_{conf})[68] arising from the solute degrees of freedom. Thus, we estimated the S_{conf} of the MMP-2/fTHP-5 complexes by the approximate formula introduced by Schlitter[69] based on a quantum mechanical one-dimensional harmonic approximation:

$$S_{\text{conf}} = \frac{1}{2} R \ln\left[\det\left(1 + \frac{k_B T e^2}{\hbar^2}\sigma'\right)\right] \quad (2)$$

where σ' is the mass-weighted covariance matrix calculated directly in terms of Cartesian coordinates of the solute atoms.[70,71] To remove the overall translation of the center of mass and the overall rotation of the protein, all the MD snapshots employed in the entropy calculations were superposed on top of each other using a least-squares fit. Schlitter's formula, which is closely related to the quasi-harmonic method,[72] is computationally very efficient, facilitating thus the estimation of the absolute entropy of large macromolecules. However, this method suffers from well-known disadvantages such as its slow convergence with sampling size and, especially, the large overestimation of S_{conf} that impedes the calculation of accurate entropy differences.[73] Hence, the Schlitter entropy can only provide insight into entropy effects at work in the equilibrium simulations of large systems.

RESULTS

MMP-2(CAT-FIB)/fTHP-5 Simulation. Insertion of the FIB domains into our former MMP-2(CAT)/fTHP-5 model as described in Methods does not result in any significant steric collapse. The FIB domains in the resulting **MMP-2(CAT-FIB)/fTHP-5** complex were allowed to accommodate the presence of fTHP-5 bound to CAT during an 85 ns MD simulation of the fully solvated complex. For this simulation, we analyzed the time evolution of the radius of gyration, the distances between the center of mass of the protein domains, and the root-mean-square deviations (rmsd) of the protein domains and selected secondary structural elements with respect to the X-ray structure (Figure S1 of the Supporting Information).

The global arrangement of the **MMP-2(CAT-FIB)/fTHP-5** model as measured by the radius of gyration remains quite stable during the simulation (22.5 ± 0.2 Å). More particularly, the internal structure of the CAT domain is hardly perturbed by the presence of FIB. Thus, the average rmsd (1.7 ± 0.1 Å) of the backbone CAT atoms is nearly identical to that derived from the MMP-2(CAT)/fTHP-5 simulation (1.8 ± 0.1 Å). The FIB1 and FIB2 subdomains show also moderate deviations with reference to the X-ray structure (1.7 ± 0.3 and 1.7 ± 0.2 Å, respectively), although FIB1 tends to slightly separate from the CAT domain whereas FIB2 approaches CAT (see Figure S1 of the Supporting Information). In contrast, the internal structure of the FIB3 subdomain, which is the closest one to fTHP-5, experiences a larger rearrangement having a rmsd value of 3.5 Å at the end of the trajectory. The three backbone chains of

DOI: 10.1021/bi501014w
Biochemistry 2015, 54, 1243−1258

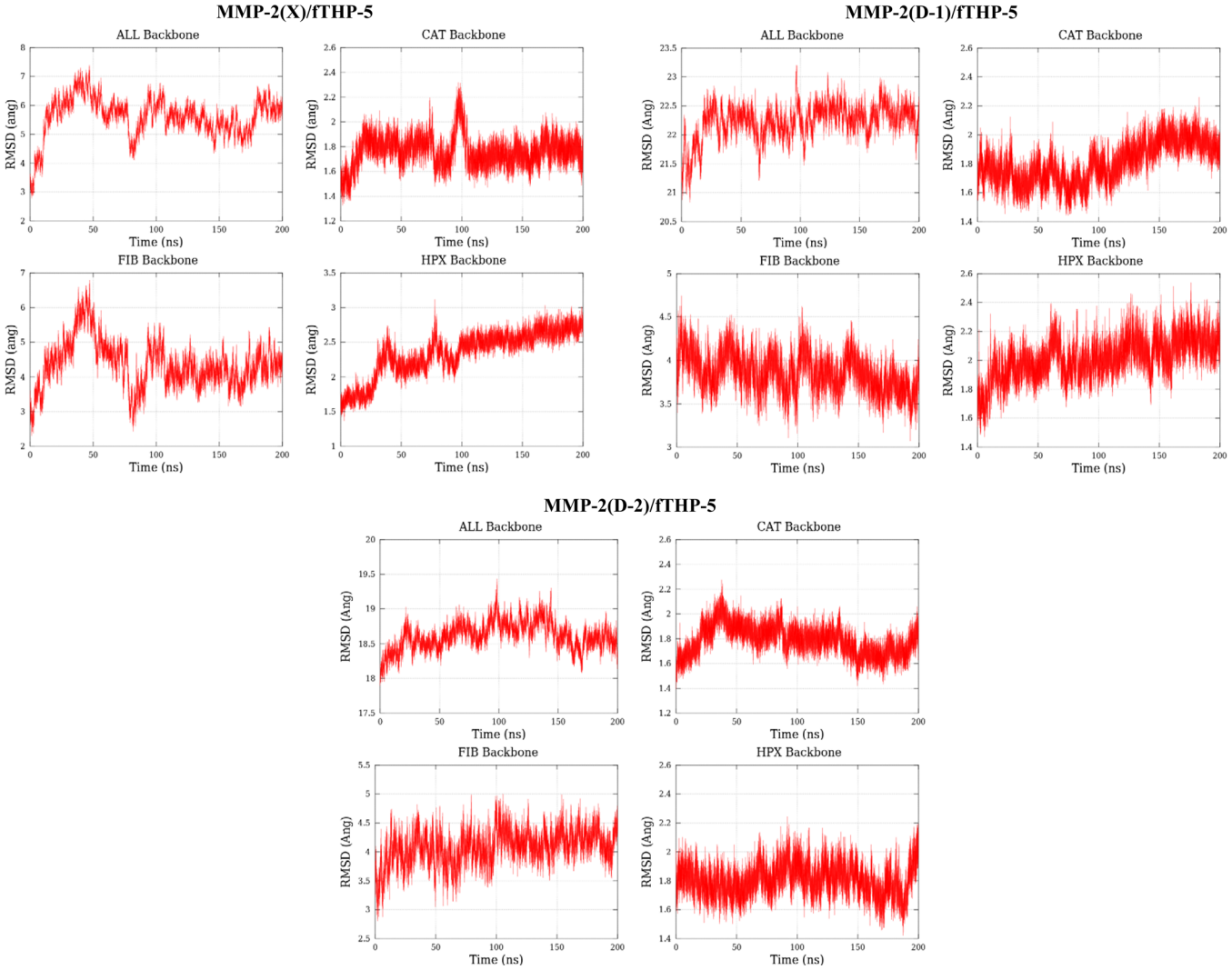

Figure 1. Time evolution along the MMP-2/fTHP-5 trajectories of the root-mean-square deviation (rmsd) computed for selected backbone heavy atoms (in angstroms).

fTHP-5 exhibit ample movements that are mainly located at the prototypical N- and C-terminal ends. The rmsd plot for the central region of the triple helix reveals a transition during the second half of the trajectory, which hardly affects the binding of chain B of fTHP-5 within the MMP-2 active site. In fact, chain B of fTHP-5 remains firmly attached to the CAT domain through hydrophobic and polar contacts similar to those described in previous work for the MMP-2(CAT)/fTHP-5 model.[35] The only noticeable change is the entrance of an additional water molecule in the active site that mediates the contact between the catalytic Zn_1 ion and the carbonyl group of the scissile peptide bond. Further analyses of this simulation were not pursued because the main purpose of the **MMP-2(CAT-FIB)/fTHP-5** trajectory was to provide a set of relaxed snapshots for building the three different configurations of the full-length MMP-2 enzyme in complex with fTHP-5 as described in Methods.

Stability of the MMP-2(FULL)/fTHP-5 Trajectories. On the basis of the MD snapshots extracted from the **MMP-2(CAT-FIB)/fTHP-5** simulation and those of the unbound full-length MMP-2 enzyme, we built three different models of the MMP-2/fTHP-5 complex using a semirigid docking protocol to add the HPX and linker regions. The models can be categorized in terms of the global arrangement of HPX with respect to the CAT-FIB domains. Thus, in the **MMP-2(X)/fTHP-5** model, HPX is initially oriented as in the 1CK7 crystal structure, but in the **MMP-2(D-1)/fTHP-5** and **MMP-2(D-2)/fTHP-5** models, HPX is placed in two alternative positions as suggested by our previous simulations.[28] However, it must be noticed that the starting situation of the HPX domain is derived from former simulations in the absence of the fTHP-5 substrate, and therefore, the relative interdomain orientation in the initial docking models corresponds most likely to a conformational state different from that intended to be sampled. For this reason, each of the three models of the full-length MMP-2 enzyme in a prereactive complex with fTHP-5 was fully relaxed by performing a 200 ns MD simulation.

Figure 1 displays the time evolution of the rmsd values corresponding to the backbone atoms of the whole MMP-2 enzyme and of the separate protein domains (CAT, FIB, and HPX). The crystallographic coordinates of 1CK7 were chosen as the reference structure, which results in large rmsd values for the whole MMP-2 protein because of the different disposition of the FIB domains and, more importantly, of the HPX domain in the D-1 and D-2 models. The rmsds of the CAT, FIB, and

DOI: 10.1021/bi501014w
Biochemistry 2015, 54, 1243−1258

HPX domains with respect to 1CK7 present lower values (~2–4 Å) that are indicative of reasonable secondary structure stability. To better assess the stability and changes undergone by each of the MMP-2 domains, the rmsd values were further segregated into distinct motifs (e.g., the Ω-loop in the CAT domain, subdomains FIB1–FIB3, etc.), and the corresponding plots are included in the Supporting Information.

The global rmsd plot in Figure 1 for the **MMP-2(X)/fTHP-5** configuration suggests that the MMP-2 multidomain arrangement changes significantly during the first half of the simulation and then reaches a structurally stable state during the last 100 ns. For the **MMP-2(X)/fTHP-5** trajectory, the global behavior of the rmsd value computed for all the backbone atoms seems to correlate with that of the whole FIB domain (see Figure 1). As the rmsd plots for the three FIB1–FIB3 subdomains (Figure S2 of the Supporting Information) are rather stable, it turns out that the intradomain reorganization among the FIB subdomains is the dominant event during the first 100 ns of the simulation. On the other hand, the segregated rmsd plots point out that the tertiary structure of HPX smoothly evolves during the second half of the simulation, which is mainly ascribed to the distortion of the HPX3 blade rather than to an interblade rearrangement (Figure S2 of the Supporting Information).

For the **MMP-2(D-1)/fTHP-5** trajectory, the global rmsd plot seems to be well equilibrated after 20 ns, but the rmsd plot for the CAT domain suggests that the search phase in this model is probably longer. Thus, we found that the conformation of the Ω-loop, which partially delimits the active site, suffers a sharp transition at ~90 ns. This transition involves a change in the configuration of the Thr_{428}-Lys_{429}-Asn_{430}-Phe_{431}-Arg_{432} backbone and results in the approach of Phe_{431}, the gatekeeper of the $S_{1'}$ pocket, to the Leu_{24B}($P_{1'}$) side chain. Finally, the rmsd plots for the **MMP-2(D-2)/fTHP-5** simulation indicate that all the structural elements evolve in equilibrium during this simulation, except the FIB2 subdomain whose rmsd value jumps from ~1.5 to ~3.0 Å at t = 100 ns (Figure S4 of the Supporting Information).

To analyze the relative position of the HPX and FIB1–FIB3 domains with respect to CAT, we monitored the evolution of the Euler angles that characterize the relative orientation of two rigid coordinate systems placed at the center of mass of the considered domains (Figures S5–S8 of the Supporting Information). Thus, the corresponding polar plots confirm that the FIB3 subdomain reorients with respect to CAT at ~100 ns during the **MMP-2(X)/fTHP-5** simulation that, in turn, induces a larger rotational motion of FIB2 (see Figures S7 and S8 of the Supporting Information). Similarly, the FIB2 and FIB3 subdomains reorient moderately at the middle of the **MMP-2(D-1)/fTHP-5** trajectory, whereas the three FIB modules remain in a stable position along the **MMP-2(D-2)/fTHP-5** simulation. No substantial rearrangement of the HPX orientation with respect to the CAT domain is observed in any of the simulations.

To further assess the stability of the trajectories, we analyzed the evolution of the approximated free energy of the solvated MMP-2 models by conducting MM-PB calculations. The $G_{MM\text{-}PB}$ energies computed for the three simulations are plotted versus time in Figure 2. For the **MMP-2(X)/fTHP-5** simulation, the wide fluctuations of the adjacent $G_{MM\text{-}PB}$ average suggest that the model relaxes from the initial conformation to a more stable conformation during the first 90–100 ns. Similarly, the accumulated $G_{MM\text{-}PB}$ average for the

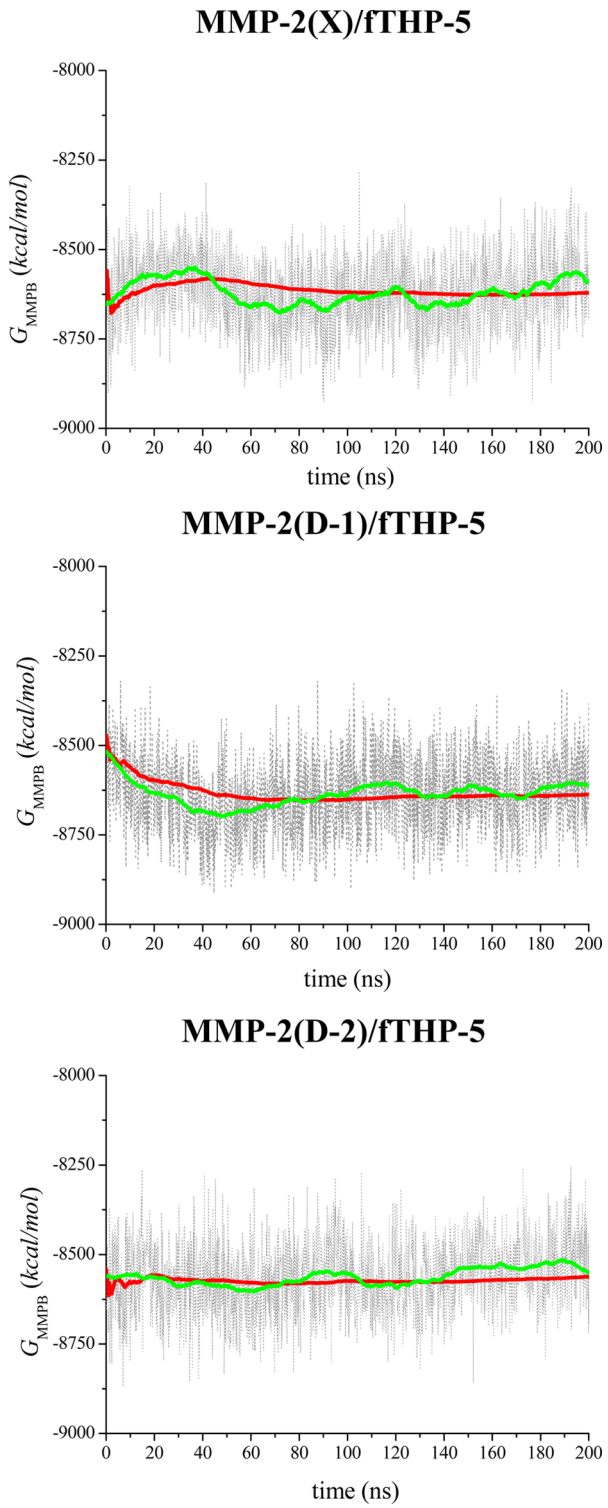

Figure 2. Solute energy plus solvation free energy ($G_{MM\text{-}PB}$) plots for the various MMP-2/fTHP-5 configurations. The gray dotted curve represents the raw data points. The red and green curves represent the evolution of the accumulated average and the adjacent average, respectively. The adjacent-average curve, which better displays the fluctuations of $G_{MM\text{-}PB}$ on the long time scale, was obtained by considering the closest 100 data points around each value along the simulation time and assuming that the $G_{MM\text{-}PB}$ plots are reflected at the two ends of the time interval.

MMP-2(D-1)/fTHP-5 model tends to decrease during the first 60–70 ns and then remains stable. It is also apparent that the

DOI: 10.1021/bi501014w
Biochemistry 2015, 54, 1243–1258

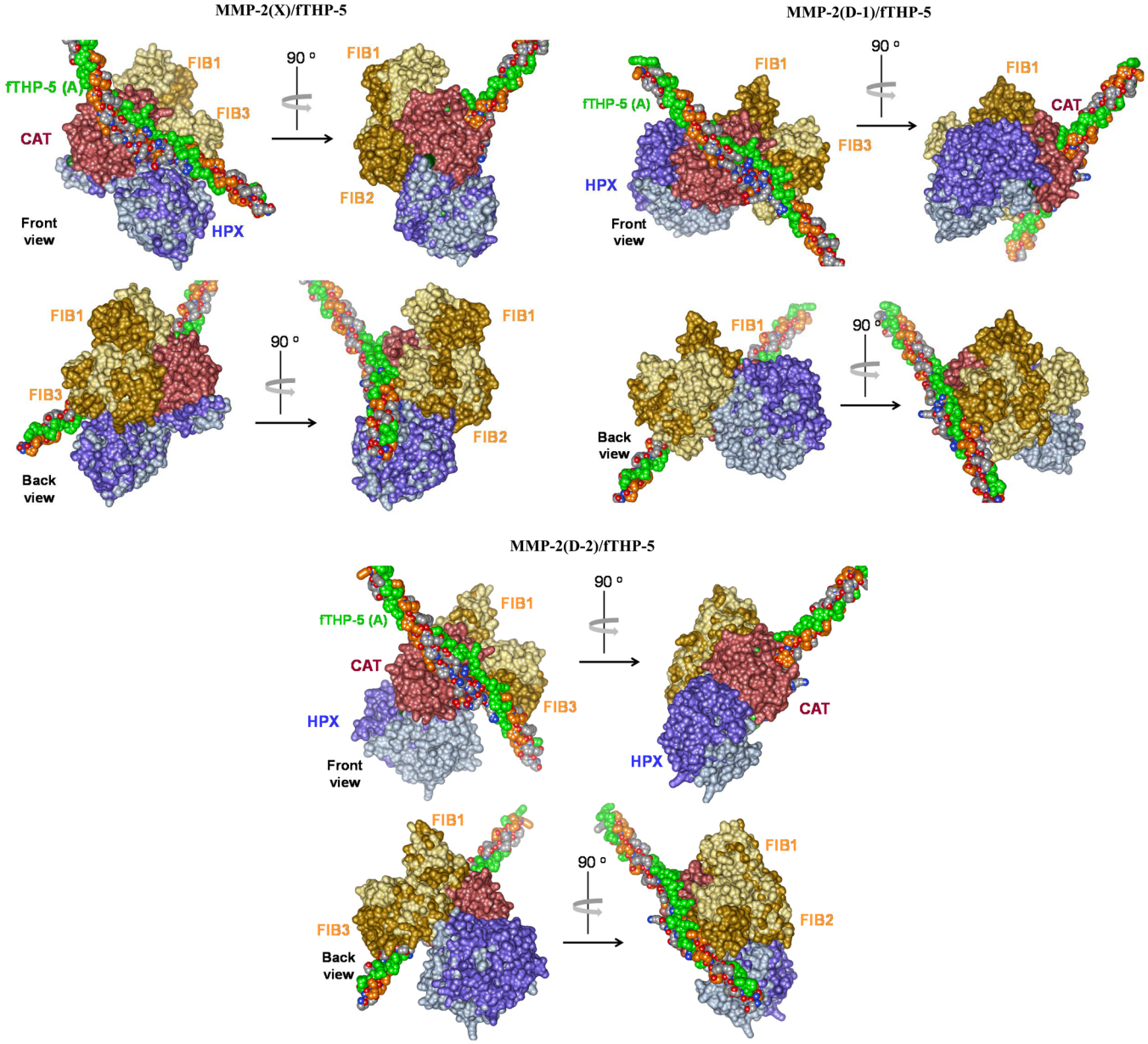

Figure 3. Different views (90° turned) for a surface representation of the average structures obtained from the last 10 ns of the MMP-2/fTHP-5 simulations. For comparison, the average structures of the HPX and FIB domains obtained from the last 10 ns of the corresponding MMP-2 simulations are also displayed in lighter colors. The MMP-2 structures were superposed over the MMP-2/fTHP-5 structures using the backbone coordinates of the CAT domain.

MMP-2(D-2)/fTHP-5 model presents a shorter relaxation phase in terms of the $G_{MM\text{-}PB}$ energies; the $G_{MM\text{-}PB}$ plot fluctuates around a stable average value after only ~30−40 ns.

When all the results are taken together, it seems that the initial placement of the HPX domain in the full-length MMP-2/fTHP-5 models generated by the semirigid docking analyses needs to be refined by tens of nanoseconds of MD simulation during which the relaxation phase of the multidomain structure in the various models is accompanied by the dampening of the increasing/decreasing trends of the structural deviations and the energetic fluctuations. Therefore, we adopted a conservative approach and decided to discard the first 100 ns of the three trajectories when conducting the rest of our statistical analyses.

Overall Structure of the MMP-2/fTHP-5 Models. Figure 3 displays a series of surface representations of the average structures obtained from the last 10 ns of the **MMP-2(X)/fTHP-5**, **MMP-2(D-1)/fTHP-5**, and **MMP-2(D-2)/fTHP-5** simulations. To help characterize the changes in the location and orientation of the HPX and FIB domains induced by the presence of the fTHP-5 triple helix bound to the CAT domain, Figure 3 also shows (in lighter colors) the positioning of the HPX and FIB domains resulting from the last 10 ns of the parent simulations of the MMP-2 enzyme in its free form.[35] In this way, the plasticity of the FIB modules upon binding of fTHP-5 becomes apparent. On one hand, in the X configuration, the FIB3 subdomain moves away from the active site cleft when fTHP-5 is bound that, in turn, also drives the reorientation of the FIB1 and FIB2 domains as suggested by the Euler plots (Figures S6−S8 of the Supporting Information). On the other hand, the rearrangement of the FIB3 subdomains in the D-1 and D-2 configurations occurs in the opposite direction, approaching the fTHP-5 substrate and

DOI: 10.1021/bi501014w
Biochemistry 2015, 54, 1243−1258

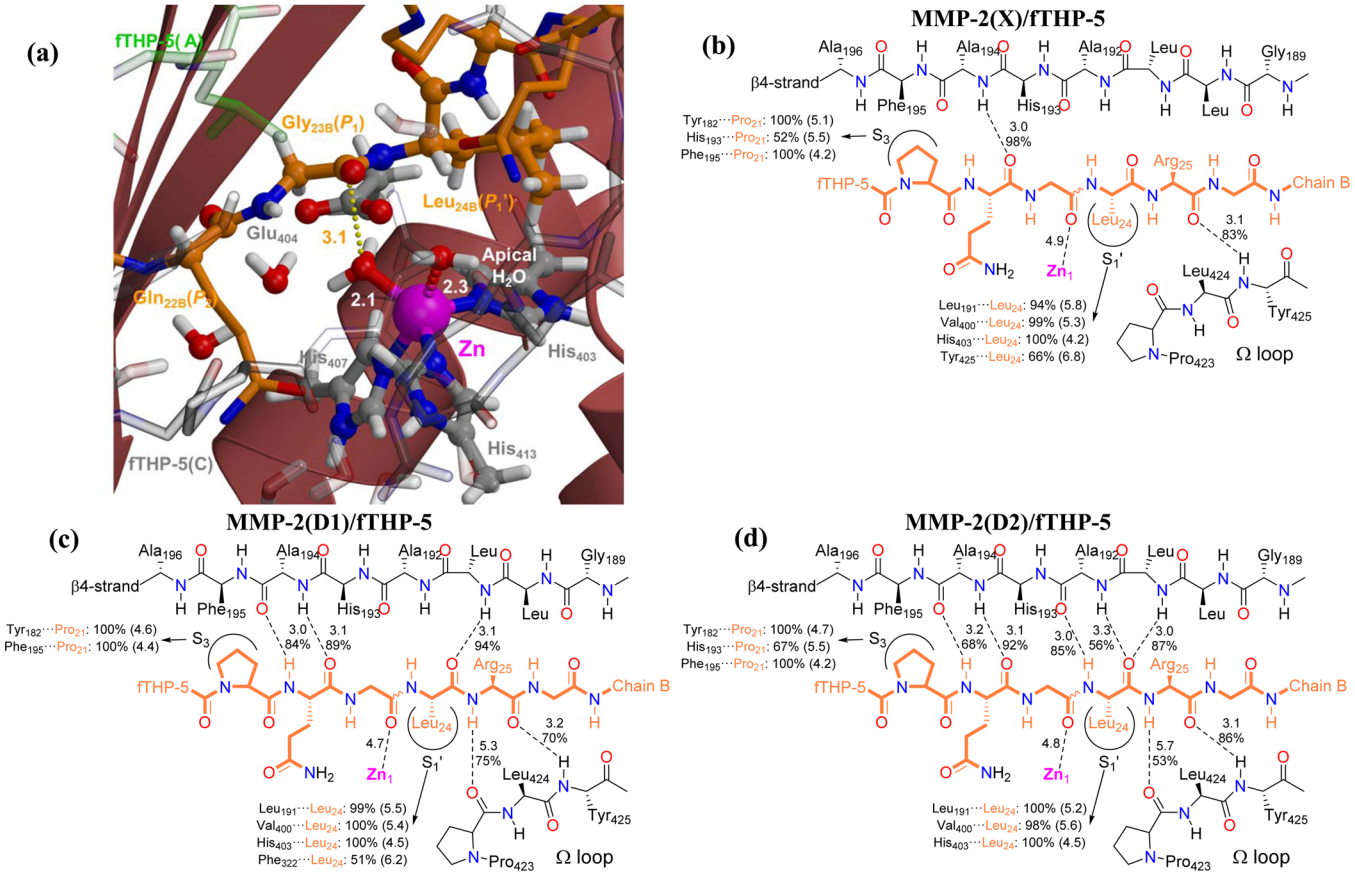

Figure 4. (a) View of the active site region of the MMP-2(X)/fTHP-5 model corresponding to the QM/MM-optimized structure derived from a representative MD snapshot. Atoms included in the QM region are shown in ball-and-stick representation. Some specific distances (in angstroms) are also indicated. (b–d) Schematic representations of the most important MMP-2···fTHP-5 interactions.

the active site region to form direct contacts with fTHP-5 (see below).

The HPX domain in the **MMP-2(X)/fTHP-5** model maintains its relative situation with respect to CAT, with only slight modifications in the average position of the HPX side chains. This lack of response could be caused by the stability of specific CAT···LNK (Gln_{435} N···Pro_{463} O, Ile_{438}···Pro_{459}, and Asp_{416} Oδ···Thr_{465} Oγ) and CAT···HPX (Tyr_{427}···Pro_{514}, Pro_{417}···Pro_{506}, and Gly_{418} O···Arg_{491} Nη) interdomain contacts that contribute to anchor HPX in a position similar to that experimentally observed in the crystal structure of proMMP-2. Curiously, in the **MMP-2(D-1)/fTHP-5** and **MMP-2(D-2)/fTHP-5** configurations, the HPX domain responds to the presence of the triple-helical peptide in spite of being placed at the rear of the CAT domain where, *a priori*, it does not interfere with the binding of substrate molecules. However, its average location changes with respect to that observed in the fTHP-5-free enzymes as shown in Figure 3. This "upward" displacement of the HPX domain is probably related to the absence of stable CAT···HPX interdomain contacts and is probably a side effect of the changes in the location of the FIB subdomains caused by fTHP-5.

With regard to the structure of the fTHP-5 ligand, we examined first the helical twist angle against sequence as averaged for the three chains (Figure S9 of the Supporting Information) and found that fTHP-5 maintains its triple-helical structure in the prototypical N- and C-terminal (Pro-Hyd-Gly) triplets. In contrast, the helix is gradually untwisted in the central region where the scissile $Gly_{23B}(P_1)$–$Leu_{24B}(P_{1'})$ peptide bond is located. Comparison with the helical twist angles computed for the MMP-2(CAT)/fTHP-5(B) trajectory shows that inclusion of the FIB and HPX domains does not modify the structure of fTHP-5 in complex with MMP-2, excepting minor variations in the average values of the twist angles in the nonprototypical region. It may be also interesting to note that the particular location of the HPX domain with respect to CAT, as sampled in the X, D-1, and D-2 models, does not perturb the untwisting of the triple helix along its sequence.

Besides the partial twisting/untwisting of the triple helix, the fTHP-5 molecule in its free form also exhibits global bending motions from linear to curved structures.[35] However, in the presence of the full-length MMP-2 enzyme, we visually detected that the triple helix adopts a bent shape (C-shaped) during the **MMP-2(X)/fTHP-5** simulation whereas it remains quite extended or adopts a slightly S-shaped form in the **MMP-2(D-1)/fTHP-5** and **MMP-2(D-2)/fTHP-5** trajectories (see the fourth view of each model in Figure 3). This observation was confirmed by conducting clustering analyses considering all the Cα atoms of the THP chains [the representative clusters obtained for the **MMP-2(X)/fTHP-5**, **MMP-2(D-1)/fTHP-5**, and **MMP-2(D-2)/fTHP-5** trajectories are shown in Figure S10 of the Supporting Information]. The clustering analyses also emphasize that the central region of the helix is quite rigid in the three simulations, as a result of the binding of chain B of fTHP-5 within the MMP-2 active site. In contrast, the N- and C-terminal tails are rather flexible, although the flexibility of the C-terminal moiety is reduced in the **MMP-2(D-2)/fTHP-5**

DOI: 10.1021/bi501014w
Biochemistry 2015, 54, 1243–1258

simulation, most probably because of its interaction with FIB3 (see below).

MMP-2···fTHP-5 Binding Interactions. The fTHP-5 molecule binds to the MMP-2 enzyme by establishing a number of polar and hydrophobic contacts. The backbone of chain B of fTHP-5 around the scissile peptide bond aligns in an extended conformation within the MMP-2 active site, and several fTHP-5 residues give stable interactions with important binding sites of the MMP-2 CAT domain situated in strand β4, the Ω-loop, and the so-called S_3 and $S_{1'}$ hydrophobic pockets (see Figure 4 and Table S1 of the Supporting Information). These MMP-2(FULL)···fTHP-5 contacts are similar to those previously observed in the MMP-2(CAT)/fTHP-5(B) model.[35] For example, in the three MMP-2/fTHP-5 simulations, the $Pro_{21B}(P_3)$ residue of fTHP-5 interacts closely with the Tyr_{182} and Phe_{195} side chains at the S_3 pocket, while $Leu_{24B}(P_{1'})$ makes contact with Leu_{191}, Val_{400}, and His_{403} side chains at the entrance of the relatively large $S_{1'}$ hydrophobic pocket. Some differences across the models can be found in the number of the most persistent (percent occupancy of >50) polar contacts [two, five, and seven contacts in **MMP-2(X)/fTHP-5**, **MMP-2(D-1)/fTHP-5**, and **MMP-2(D-2)/fTHP-5**, respectively], which reflect a slightly different arrangement of the fTHP-5 substrate within the active site (see Figure 4).

A particular characteristic of the fTHP-5 binding mode in the MMP-2/fTHP-5 complexes is related to the entry of one or two water molecules in the vicinity of the catalytic Zn_1 ion that mediate the contact between Zn_1 and the carbonyl group of $Gly_{23B}(P_1)$, instead of the direct Zn_1···O=C interaction observed between the CAT domain of MMP-2 and small peptide substrates.[9] As mentioned in Methods, the apical coordination position around the Zn_1 ion occupied either by the Gly_{23B} carbonyl or by the incoming water is described by nonbonded parameters, allowing thus the ligand exchange at this position during the MD simulation. To further characterize the structure of the Zn_1 site in the presence of fTHP-5, we conducted a QM/MM optimization of a representative snapshot extracted from the **MMP-2(X)/fTHP-5** trajectory at t = 100 ns (see Figure 4a) in which the Zn_1 ion and its ligands, the $Gly_{23B}(P_1)$−$Leu_{24B}(P_{1'})$ moiety, and the nearby water molecules are included in the QM region. The optimized QM/MM structure shows interatomic distances and angles that are very similar to those observed during the MD simulation (see the Supporting Information for details), showing thus that the structure of the Zn_1 complex sampled by the MD simulations corresponds to a stable coordination environment and is likely not an artifact of the MM parametrization. Furthermore, the QM/MM structure and the MD data indicate that the presence of the water-bridged $Gly_{23B}(P_1)$ C=O···$(H_2O)_{1-2}$···Zn_1 interactions probably enhance the prereactive character of the MMP-2/fTHP-5 complex. For example, as seen in Figure 4a, the orientation of the $Gly_{23B}(P_1)$−$Leu_{24B}(P_{1'})$ amide linkage is adequate for the nucleophilic attack of the metal-bound O atom in the Zn_1−(H_2O)···$^-$OOC−Glu_{404} moiety toward the C atom of $Gly_{23B}(P_1)$ (e.g., the MD Zn−O···C=O average distance amounts to 3.3 ± 0.2 Å for the X and D-1 models and 3.1 Å in the QM/MM-optimized model) following a reaction pathway with assistance of the Glu_{404} carboxylate similar to that determined computationally for the hydrolysis of a decapeptide catalyzed by MMP-2.[8]

Besides the key interactions associated with the placement of chain B of fTHP-5 within the narrow MMP-2 active site, other fTHP-5 residues in its chain A also make statistically relevant contacts with the MMP-2 CAT domain in the three sampled MMP-2/fTHP-5 models (Table S1 of the Supporting Information). These contacts involve substrate residues from P_5 (Amp_{19A}), which interacts with Tyr_{182} and Phe_{195} outside the S_3 pocket, to $P_{5'}$ (Dnp_{28A}), which contacts Tyr_{395} at the connection between CAT and FIB3. We also observed highly abundant interactions between CAT and chain C in the **MMP-2(D-1)/fTHP-5** and **MMP-2(D-2)/fTHP-5** models, but not for the **MMP-2(X)/fTHP-5** model.

A few interactions between some fTHP-5 residues and the noncatalytic domains (i.e., HPX and FIB) have been detected, although their precise identity is different for each MMP-2/fTHP-5 model. For the **MMP-2(X)/fTHP-5** simulation, these contacts are scarce and mainly limited to the hydrophobic interaction between the nonstandard residue Dnp in chains B and C and residues Met_{504} and Leu_{507} located in the first blade of the HPX domain (84−94% occupancy). Other less abundant HPX···fTHP-5 contacts are Gly_{483} O···$Arg_{31C}(P_{8'})$ Nη with a frequency of 40%, Arg_{482} O···$Arg_{31B}(P_{8'})$ Nη and Glu_{484} Oε··· $Arg_{31C}(P_{8'})$ Nε with a frequency of 15%, Arg_{482} O··· $Hyp_{34B}(P_{11'})$ Oγ with a frequency of 12%, and Phe_{512}··· $Dnp_{28B}(P_{5'})$ with a frequency of 13%. In contrast, in the **MMP-2(D-1)/fTHP-5** and **MMP-2(D-2)/fTHP-5** models, the FIB3 subdomain is the only MMP-2 domain apart from CAT that is adequately placed to interact directly with the fTHP-5 substrate. During the last 100 ns of the **MMP-2(D-1)/fTHP-5** simulation, we observed abundant polar interactions [Cys_{363} O···$Hyp_{34B}(P_{11'})$ Oγ (85%), Asp_{392} Oδ···$Arg_{31B}(P_{8'})$ Nη (66%), and Arg_{368} O···$Arg_{31A}(P_{8'})$ Nη (53%) (Table S1 of the Supporting Information)] and hydrophobic contacts [Met_{373}···$Val_{30B}(P_{7'})$ (78%), Met_{373}···$Pro_{33C}(P_{10'})$ (46%), and Tyr_{360}···$Hyp_{34B}(P_{11'})$ (32%)]. The same FIB3 sites interact with $Pro_{33C}(P_{10'})$ and $Pro_{36C}(P_{13'})$ in the **MMP-2(D-2)/fTHP-5** model.

To complement the information provided by the analyses of the H-bond and vdW contacts, we also analyzed the PB electrostatic potential mapped onto the solvent-excluded molecular surface area of selected MD snapshots (see Figure 5). Perhaps the most remarkable observation is that the fTHP-5 region around the scissile peptide bonds, which exhibits a local concentration of positive charge because of the presence of Arg residues at the $P_{2'}$ and $P_{8'}$ locations amid neutral fTHP-5 residues, is electrostatically stabilized by the predominantly negative potential over the THP-contacting surface of the MMP-2 CAT and FIB domains. Hence, the combined surface of the CAT and FIB domains seems to "solvate" specifically the fTHP-5 region that mimics the segment of the α chain of collagen type II that is recognized by the MMPs.

Energetic Analyses. The average values of the $G_{MM\text{-}PB}$ energy terms for the MMP2/fTHP-5 complexes and their standard errors are reported in Table 1 considering only the last 100 ns of each trajectory. As seen in Figure 2, the $G_{MM\text{-}PB}$ energies oscillate rapidly on the subnanosecond time scale, but they also exhibit lower-amplitude oscillations on longer time scales as shown by the evolution of the adjacent averages. This suggests that the $G_{MM\text{-}PB}$ energetic terms behave as correlated fluctuating quantities, and therefore, we also estimated the error of their average values by means of block averaging.[74] Table 1 also collects the MM-PB data for the unbound states of the MMP-2 and fTHP-5 molecules, which are useful for performing comparative analyses and estimating the binding energy of the complexes.

DOI: 10.1021/bi501014w
Biochemistry 2015, 54, 1243−1258

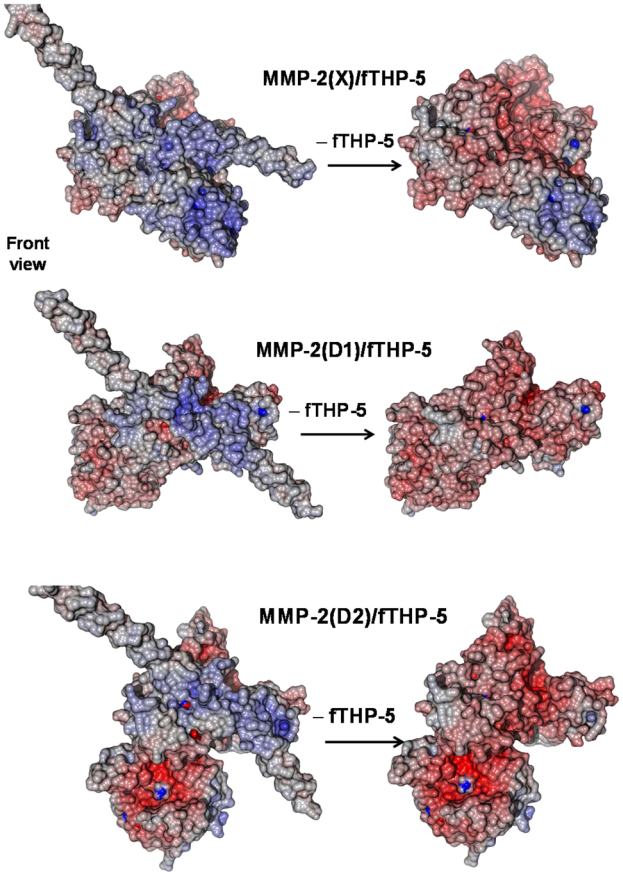

Figure 5. Electrostatic potential mapped onto the molecular surface of representative MD snapshots extracted from the MMP-2/fTHP5 simulations. The calculations were performed both in the full MMP-2/fTHP5 models including the coordinates of the triple helix (left) and in the MMP-2 models after the fTHP-5 substrate had been removed (right). Red indicates negative potential and blue positive potential.

To rank the X, D-1, and D-2 configurations of the MMP-2/fTHP-5 complexes according to their relative stability, we combine the average $G_{\text{MM-PB}}$ values of the respective simulations. Thus, the **MMP-2(D-1)/fTHP-5** model would be more stable than the **MMP-2(X)/fTHP-5** and **MMP-2(D-2)/fTHP-5** models by +1 and +72 kcal/mol, respectively. However, the propagation of the standard error (*se*) or the block-averaging error (*be*) estimate associated with the individual energy terms results in large statistical uncertainties for these ΔG differences: 4.5 and 4.4 kcal/mol (*se*) and 14.9 and 15.2 kcal/mol (*be*), respectively. Therefore, we cannot discriminate between the **MMP-2(X)/fTHP-5** and **MMP-2(D-1)/fTHP-5** states because their relative ΔG is much smaller than the statistical uncertainty. In contrast, the **MMP-2(D-2)/fTHP-5** state can be safely ruled out as being accessible to the MMP-2/fTHP-5 complex because the corresponding ΔG is much larger than either the *se* or the *be*. Curiously, it turns out that the binding of fTHP-5 contributes to destabilize specifically the positioning of the HPX domain in the D-2 orientation given that the native MMP-2(D-2) model is scored by only ∼15 kcal/mol above D-1 using an equivalent MM-PB approach.[28] On the other hand, it is not unreasonable to expect that the **MMP-2(X)/fTHP-5** and **MMP-2(D-1)/fTHP-5** models have a similar stability because (a) in the absence of fTHP-5, the results of comparable MM-PB analyses[28] point out again that the parent models are energetically alike and (b) either the HPX domain in **MMP-2(X)/fTHP-5** or the FIB3 subdomain in **MMP-2(D-1)/fTHP-5** gives only weak to moderate interactions with the fTHP-5 substrate.

To better characterize the relative stability of the MMP-2/fTHP-5 models, we also analyzed their absolute configurational entropy (S_{conf}) by means of the Schlitter approximation. Thus, we computed the plots of S_{conf} versus simulation time during the last 100 ns for the whole MMP-2/fTHP-5 systems or its various protein domains (Figure S11 of the Supporting Information). The S_{conf} limiting values for the three models after accumulated sampling for 100 ns are close to each other: 35.5, 35.6, and 35.4 kcal mol^{-1} K^{-1} for the X, D-1, and D-2 models, respectively (the S_{conf} values of the three parent models in the native MMP-2 form are also quite similar). Although these entropy calculations are rather approximate because of the limited sampling size and the well-known overestimation of S_{conf} by Schlitter's method, the similarity of the S_{conf} plots suggests that the inter- and intradomain mobility of the MMP-2/fTHP-5 models should have only a minor entropic impact on their relative stability.

Finally, we estimated the binding energy ($\Delta_{\text{bind}}G$) by combining the average $G_{\text{MM-PB}}$ terms from the independent MD trajectories for the complexes, the native triple-helical state of the fTHP-5 protein,[35] and the three MD trajectories of the unbound form of full-length MMP-2 in the X, D-1, and D-2

Table 1. Average Values for the MM-PB Energy Components (in kilocalories per mole) from the MMP-2/fTHP-5 MD Simulations (last 100 ns) Reported in This Work, the MD Simulations of the Isolated MMP-2 (last 100 ns) in the X, D-1, and D-2 Orientations, and the fTHP-5 System (last 40 ns)[a]

system	$\overline{E}_{\text{MM}}$	$\Delta\overline{G}^{\text{PB}}_{\text{solv}}$	$\Delta\overline{G}^{\text{nonpolar}}_{\text{solv}}$	$\overline{G}_{\text{MM-PB}}$
MMP-2(X)/fTHP-5	−1969.1 (5.0) [34.5]	−7316.4 (4.3) [32.9]	661.5 (1.6) [2.1]	−8622.2 (3.2) [13.1]
MMP-2(D-1)/fTHP-5	−2175.4 (5.4) [35.5]	−7123.8 (4.5) [34.0]	674.3 (1.6) [4.7]	−8623.1 (3.2) [7.1]
MMP-2(D-2)/fTHP-5	−2274.3 (5.2) [30.2]	−6972.7 (4.2) [21.8]	694.1 (1.5) [2.8]	−8551.2 (3.0) [13.4]
fTHP-5[b]	1455.9 (1.4) [2.8]	−1336.2 (0.7) [2.7]	−37.8 (0.7) [3.0]	83.2 (1.2) [5.2]
MMP-2-(X)[b]	−2624.6 (3.3) [31.6]	−6667.2 (2.8) [30.6]	611.4 (1.0) [3.8]	−8680.2 (1.9) [7.7]
MMP-2-(D-1)[b]	−2779.2 (3.6) [36.0]	−6529.2 (3.1) [35.9]	623.0 (1.0) [3.0]	−8685.7 (2.1) [11.6]
MMP-2-(D-2)[b]	−2936.0 (3.5) [43.8]	−6364.3 (2.8) [36.5]	629.1 (1.1) [5.2]	−8671.6 (2.0) [12.7]
MMP-2(X) + fTHP-5 → MMP-2(X)/fTHP-5	−800.4 (6.2) [46.9]	687.0 (5.2) [45.0]	87.9 (2.9) [5.3]	−25.2 (3.9) [16.1]
MMP-2(D-1) + fTHP-5 → MMP-2(D-1)/fTHP-5	−852.1 (6.6) [46.9]	741.6 (5.5) [49.5]	89.1 (2.0) [6.3]	−20.6 (4.0) [14.6]
MMP-2(D-2) + fTHP-5 → MMP-2(D-2)/fTHP-5	−794.2 (6.6) [53.3]	727.5 (5.1) [42.6]	102.8 (2.0) [6.6]	37.2 (3.8) [19.2]

[a]Relative MM-PB energies for the complex formation are also included. Standard errors of the mean values and block average error estimates are given in parentheses and brackets, respectively. [b]Calculated using the snapshots of MD simulations reported previously.[28,35]

DOI: 10.1021/bi501014w
Biochemistry 2015, 54, 1243−1258

orientations.[28] The resulting $\Delta_{bind}G$ values are −25, −21, and +37 kcal/mol for the X, D-1, and D-2 configurations, respectively (see Table 1). Perhaps the most interesting observation arising from the $\Delta_{bind}G$ estimations is that the formation of the **MMP-2(X)/fTHP-5** and **MMP-2(D-1)/fTHP-5** complexes would be thermodynamically favorable (i.e., $\Delta_{bind}G < 0$), supporting thus the stability and relevance of these computational models. As expected, the electrostatic and dispersion forces between the two proteins provide the driving force for the formation of the complex. For example, the $\Delta\overline{E}_{MM}$ change for the binding process leading to **MMP-2(X)/fTHP-5** has a value of approximately −800 kcal/mol, which compensates for the desolvation penalty for binding measured by the $\Delta\Delta\overline{G}^{PB}_{solv}$ and $\Delta\Delta\overline{G}^{nonpolar}_{solv}$ values of +687 and +88 kcal/mol, respectively. Unfortunately, the large magnitude of the $\Delta\overline{E}_{MM}$ and $\Delta\Delta\overline{G}_{solv}$ values and their ample fluctuations, which are a consequence of the relatively large size of the molecular fragments involved in the binding process and the broad contact area between them, limit the accuracy and precision of the MM-PB estimations of protein−protein binding energies. In fact, the actual values of the MM-PB binding energies in Table 1 should be taken with caution because of the limitations of the MM-PB method, the lack of entropic contributions, and the large statistical uncertainty of the computed values, which lies in the interval of ∼4−16 kcal/mol depending on the error estimation considered (standard error or block averaging error).

DISCUSSION

In spite of its physiological and pathological relevance, we still lack detailed structural information about the enzyme/substrate interactions operating in the collagen hydrolysis catalyzed by the MMPs. This has prompted us to analyze three different models for the interaction of the ubiquitous full-length MMP-2 enzyme with the synthetic collagen-like fTHP-5 in a prereactive state, in which the triple helix is partially unfolded and the scissile peptide in chain B of the THP is placed within the Zn_1 active site. It may be interesting to remark that, because of the structural and dynamical complexity of the two biomolecules, the construction of the MMP-2/fTHP-5 complex is far from being a straightforward molecular modeling task. In fact, the initial structures of such complexes can be accessed only by relying heavily on the previous structural knowledge that has been acquired through a continuous effort focused on the computational study of the MMP-2 enzyme.[8−10,28,35,40,75] Subsequently, the obtained MMP-2/fTHP-5 models are subject to extensive MD simulations in explicit solvent that are indispensable for the proper relaxation of the MMP-2 interdomain arrangement and the MMP-2···fTHP-5 mutual orientation through collective motions on the nanosecond time scale. Thus, the final MMP-2/fTHP-5 models comprise an ensemble of structures that are extracted from the second half of the 200 ns MD trajectories.

With regard to the stability of the MMP-2/fTHP5 complexes, the structural analyses of the MD trajectories confirmed that the partially unfolded fTHP-5 substrate remains well anchored to the enzyme, mainly through polar and hydrophobic interactions located along the active site cleft of CAT as described in the legend of Figure 4. The identity and average distances of some of these interactions vary across the models, a fact that seems to be associated with the reorientation of the hydrolyzable peptide bond as a result of the entrance of one or two water molecules that mediate the Zn_1···O $Gly_{23B}(P_1)$ contact. However, in the three models, the scissile $Gly_{23B}(P_1)$−$Leu_{24B}(P_{1'})$ amide bond remains well oriented to react with the catalytic machinery of the enzyme (i.e., the zinc-bound water molecule and the conserved Glu_{404}).[8] Hence, the ability of the various models to represent the equilibrium state of the MMP-2/fTHP-5 complex needs to be further assessed in terms of their average MM-PB energies and configurational entropies (see Table 1). Although these energetic analyses yield approximate free energies, they allow us to safely discard the **MMP-2(D-2)/fTHP-5** model, which is much less stable than the **MMP-2(X)/fTHP-5** and **MMP-2(D-2)/fTHP-5** configurations. The MM-PB energy difference between the latter models is smaller than the corresponding statistical uncertainty, and accordingly, the two of them are *a priori* reasonable candidates for describing the prereactive MMP-2/fTHP-5 complex.

The most likely models mainly differ in the positioning of the HPX domain with respect to CAT. In the **MMP-2(X)/fTHP-5** model, HPX is close to the catalytic site cleft as in the available crystal structures of pro-MMP-2 while HPX is located at the rear of CAT and distal to the active site groove during the **MMP-2(D-1)/fTHP-5** simulation. The fact that these models have similar MM-PB energies and limiting S_{conf} values can be seen as an indication that the HPX domain could sample different configurations in the prereactive MMP-2/THP complexes. In addition, it turns out that the FIB modules also undergo a notable rearrangement in their average location and relative orientation in response to the presence of the bound fTHP-5 substrate (see Figure 2). Thus, the structure and relative stability of the computational models highlight the plasticity of the multidomain MMP-2 enzyme, in which the FIB and HPX domains could adopt distinct conformational states around CAT. This observation is in line with a variable degree of interdomain flexibility that has been invoked in previous works to explain the initial events in the collagenolysis catalyzed by the MMPs.[18,76] Thus, conformational freedom between the different domains is considered to be important for displacing the MMPs along collagen fibrils and for unwinding and/or perturbing the triple helix to accommodate a single peptide chain in the active site. Evidence confirming this interdomain flexibility has been obtained for a number of MMPs using different experimental[22−26] and computational techniques.[28,40,77] Unfortunately, gaining more detailed knowledge about the extent and significance of the MMP-2 interdomain freedom and its role during collagenolysis will require a considerable amount of MD sampling and/or the application of sophisticated meta-dynamics techniques, because of the large number of degrees of freedom and the long time scales involved in the collective motions of the MMP-2 domains. In addition, the substantial relaxation experienced by our initial docking models during the MD trajectories also suggests that other computational approaches based on semirigid docking protocols are unlikely to unveil all the details related to the plasticity of MMP-2.

For the MMP-2 enzyme, the actual role of its noncatalytic domains in THP binding and the identity of the collagen binding domain still remain controversial given that both FIB and HPX have been involved in the interaction of MMP-2 with other macromolecules. On one hand, it has been shown that an MMP-2 mutant lacking HPX is unable to cleave collagen type I fibrils, whereas the MMP-2 mutant lacking FIB generates the classical 1/4 and 3/4 cleavage products.[15] Thus, the specific collagenolysis performed by MMP-2 is seemingly determined

DOI: 10.1021/bi501014w
Biochemistry 2015, 54, 1243−1258

by HPX, not by FIB. On the other hand, it has also been reported that a FIB deletion mutant of proMMP-2 (inactivated by the propeptide) fails to bind type I collagen, whereas binding is observed for the wild type and the HPX deletion mutant proenzymes.[78] In line with this result, a variety of studies have concluded that virtually all the collagen binding properties of MMP-2 reside in the FIB domains.[5,31,79] Very recently, several MMP-2/THP complexes have been built by means of docking calculations and MD simulations.[77] In these complexes, the THP molecules are forced to interact simultaneously with a group of residues from the three FIB modules; that is, the resulting complexes are not catalytically relevant given that the active site of the CAT domain remains unoccupied. Although the HPX domain does not interact with the THP moieties either, the authors of this computational study[77] have proposed on the basis of approximate normal mode analyses that a significant displacement of HPX could allow it to interact with the THP to prevent further unwinding. Regardless of the adequacy of the constraints imposed in this study, which may be questionable, it still remains unclear how the CAT domain finally reorients itself to contact and hydrolyze the partially unwound substrate. In contrast, our MMP-2/fTHP-5 models, with a partially unfolded triple helix aligned parallel to the enzyme active site groove and its middle α chain ready to be broken, may provide a first glimpse of the important contacts in the prereactive state.

Certainly, our computational models of the MMP-2/fTHP-5 complex cannot answer all the open questions and puzzles regarding the collagen binding properties of MMP-2 due to the limited sampling achieved by the simulations and, especially, the fact that the synthetic fTHP-5 molecules have a triple helix much shorter than that of natural collagen molecules and less amino acid diversity than natural collagen molecules. Nevertheless, our calculations can give new insight into the potential role of HPX/FIB and/or help clarify some of the experimental observations. For example, we found that the direct interactions of fTHP-5 with the noncatalytic domains are limited to a few polar and hydrophobic contacts with FIB3 in the **MMP-2(D-1)/fTHP-5** model, and with HPX in the **MMP-2(X)/fTHP-5** trajectory. However, our structural analyses also show that the FIB3···fTHP-5 and HPX···fTHP-5 contacts represent a minor contribution to substrate binding in the prereactive state and that the MMP-2 CAT domain is indeed the most important binding partner for the fTHP-5 substrate. This seems to be in full agreement with experimental data showing that the isolated CAT domain of MMP-1, MMP-3, MMP-9, MMP-12, and MMP-14 can bind and process synthetic collagen models.[80−85] Therefore, it might well be that, for synthetic THP systems comprising only a few triplets of residues mimicking natural collagen sequences around the scissile peptide bond, the HPX and FIB modules would have an only minor effect as suggested by our theoretical models.

Despite the secondary role of the noncatalytic MMP-2 domains for anchoring the fTHP-5 system, the binding exosites detected in our simulations are compatible with previous experimental results obtained for other members of the MMP family. For instance, binding sites equivalent to those highlighted by mutagenesis experiments [Arg_{272} and Phe_{301} (MMP-1 numbering)] and those observed in the crystal structure of MMP-1 bound to a THP in a nonproductive way [Arg_{272}···$Hyp_B(P_{11'})$ CO, Glu_{274}···$Hyp_B(P_{11'})$ Oγ, and Phe_{301}···$Leu_B(P_{10'})$] are also involved in the interaction of HPX with fTHP-5 along the **MMP-2(X)/fTHP-5** simulation [Arg_{482} O··· $Arg_{31B}(P_{8'})$ Nη, Arg_{482} O···$Hyp_{34B}(P_{11'})$ Oγ, Glu_{484} Oε··· $Arg_{31C}(P_{8'})$ Nε, and Phe_{512}···$Dnp_{28B}(P_{5'})$ (MMP-2 numbering)].[19,20] The low percentages of abundance (13−15%) obtained for these HPX···fTHP-5 interactions are most likely due to the presence of the non-natural and bulky Dnp residue at $P_{5'}$ and of the five prototypical triplets (Gly-Pro-Hyp) from $P_{9'}$ to $P_{23'}$ in the fTHP-5 sequence. In fact, as previously noted, the HPX domain becomes more significant for facilitating proteolysis when the THP substrate becomes longer and more "collagen-like".[19] With respect to the FIB exosites, our simulations show that only FIB3 is able to make a direct contact with the fTHP-5 triple helix in the prereactive state. Previous binding analyses have localized the gelatin binding pocket of FIB3 around residues Phe_{355}, Trp_{374}, Tyr_{381}, and Trp_{387}, whereas the pro-MMP-2 crystal structure shows that the Phe_{37} residue from the propetide binds within the FIB3 hydrophobic pocket.[33,34,37] In the **MMP-2(D-1)/fTHP-5** model, none of the fTHP-5 residues directly binds within the FIB3 gelatin binding site, but a quite stable Met_{373}···$Val_{30B}(P_{7'})$ contact and a less frequent Tyr_{360}···$Hyp_{34B}(P_{11'})$ interaction are observed in the same region of the FIB3 module. Again, the sequence of the fTHP-5 substrate could not be adequate for properly exploring the binding determinants within the FIB3 exosite.

In summary, the semirigid docking calculations have processed the structural and dynamical information retrieved from previous simulations of the full-length MMP-2 enzyme and the MMP-2(CAT)/fTHP-5 complex to build realistic models of the multidomain MMP-2/fTHP-5 complex in its prereactive state. The two most important models, which were validated through MD simulations and scrutinized by different structural and energetic analyses, indicate that the HPX domain, either in its front or in its rear location with respect to CAT, and the FIB subdomains all respond to the presence of the fTHP-5 substrate by substantially changing their relative interdomain positioning. However, the simulations strongly suggest that the HPX and FIB domains can have an only minor role in substrate binding and catalysis of synthetic THP systems. Interestingly, they also pinpoint a few binding exosites in HPX and in the FIB3 module involving MMP-2 residues that coincide with some of the MMP exosites that have been determined experimentally. This favorable comparison, which augments the overall reliability of the present simulations, points out that the full-length MMP-2/fTHP-5 models would constitute the natural starting basis for further computational studies aimed at unraveling the many structural and dynamical questions concerning the role of the HPX and FIB domains in their interaction with natural collagen. Surely, this would be a genuine *tour de force* for molecular modeling methodologies because of not only the multidomain structure and flexibility of MMP-2 but also the presumably complex behavior of collagen.

■ ASSOCIATED CONTENT

Supporting Information

Time evolution during the MD simulations of the radius of gyration, segregated rmsd values, and selected interatomic distances (Figures S1−S4), dial plots of the Euler rotational angles of the HPX and FIB subdomains with respect to CAT (Figures S5−S8), measured helical twist angles along the fTHP-5 sequence (Figure S9), ribbon models of cluster representatives of the fTHP-5 molecule bound to MMP-2 (Figure S10), convergence plots of configurational entropy (Figure S11), average distances and abundance of the main

DOI: 10.1021/bi501014w
Biochemistry 2015, 54, 1243−1258

contacts between MMP-2 and fTHP-5 (Table S1), ball-and-stick model of the QM region in the QM/MM-optimized structure of the MMP-2(X)/fTHP-5 complex (Figure S12), comparison of selected distances and angles between the QM/MM and MM structures (Table S2), and PQR files for the protein atoms and a 12.0 Å thick solvent layer extracted from the last snapshots of the **MMP-2(X)/fTHP-5** and **MMP-2(D-1)/fTHP-5** simulations. This material is available free of charge via the Internet at http://pubs.acs.org.

AUTHOR INFORMATION

Corresponding Author

*E-mail: diazfnatalia@uniovi.es. Telephone: +34-985103468. Fax: +34-985103125.

Funding

This research was initiated under the support of Grant CTQ2007-63266 (MEC, Spain).

Notes

The authors declare no competing financial interest.

REFERENCES

(1) McCawley, L. J., and Matrisian, L. M. (2001) Matrix metalloproteinases: They're not just for matrix anymore! *Curr. Opin. Cell Biol. 13*, 534−540.

(2) Butler, G. S., and Overall, C. M. (2009) Updated biological roles for matrix metalloproteinases and new "intracellular" substrates revealed by degradomics. *Biochemistry 48*, 10830−10845.

(3) Rodríguez, D., Morrison, C. J., and Overall, C. M. (2010) Matrix metalloproteinases: What do they not do? New substrates and biological roles identified by murine models and proteomics. *Biochim. Biophys. Acta 1803*, 39−54.

(4) Overall, C. M., and Kleifeld, O. (2006) Validating matrix metalloproteinases as drug targets and anti-targets for cancer therapy. *Nat. Rev. Cancer 6*, 227−239.

(5) Overall, C. M. (2002) Molecular determinants of metalloproteinase substrate specificity. *Mol. Biotechnol. 22*, 51−86.

(6) Maskos, K. (2005) Crystal structures of MMPs in complex with physiological and pharmacological inhibitors. *Biochimie 87*, 249−263.

(7) Tallant, C., Marrero, A., and Gomis-Rüth, F. X. (2010) Matrix metalloproteinases: Fold and function of their catalytic domains. *Biochim. Biophys. Acta 1803*, 20−28.

(8) Díaz, N., and Suárez, D. (2008) Peptide hydrolysis catalyzed by matrix metalloproteinase 2: A computational study. *J. Phys. Chem. B 112*, 8412−8424.

(9) Díaz, N., Suárez, D., and Suárez, E. (2010) Kinetic and binding effects in peptide substrate selectivity of matrix metalloproteinase-2: Molecular dynamics and QM/MM calculation. *Proteins 78*, 1−11.

(10) Díaz, N., and Suárez, D. (2007) Molecular dynamics simulations of matrix metalloproteinase 2: Role of the structural metal ions. *Biochemistry 46*, 8943−8952.

(11) Bode, W. (1995) A helping hand for collagenases: The haemopexin-like domain. *Structure 3*, 527−530.

(12) Piccard, H., Van den Steen, P. E., and Opdenakker, G. (2007) Hemopexin domains as multifunctional liganding modules in matrix metalloproteinases and other proteins. *J. Leukocyte Biol. 81*, 870−892.

(13) Murphy, G., Allan, J. A., Willenbrock, F., Cockett, M. I., O'Connell, J. P., and Docherty, A. J. P. (1992) The role of the C-terminal domain in collagenase and stromelysin specificity. *J. Biol. Chem. 267*, 9612−9618.

(14) Knäuper, V., Cowell, S., Smith, B., López-Otin, C., O'Shea, M., Morris, H., Luciano Zardi, L., and Murphy, G. (1997) The role of the C-terminal domain of human collagenase-3 (MMP-13) in the activation of procollagenase-3, substrate specificity, and tissue inhibitor of metalloproteinase interaction. *J. Biol. Chem. 272*, 7608−7616.

(15) Patterson, M. L., Atkinson, S. J., Knäuper, V., and Murphy, G. (2001) Specific collagenolysis by gelatinase A, MMP-2, is determined by the hemopexin domain and not the fibronectin-like domain. *FEBS Lett. 503*, 158−162.

(16) Tam, E. M., Moore, T. R., Butler, G. S., and Overall, C. M. (2004) Characterization of the distinct collagen binding, helicase and cleavage mechanisms of matrix metalloproteinase 2 and 14 (Gelatinase A and MT1-MMP). *J. Biol. Chem. 279*, 43336−43344.

(17) Brodsky, B., Thiagarajan, G., Madhan, B., and Kar, K. (2008) Triple-helical peptides: An approach to collagen conformation, stability, and self-association. *Biopolymers 89*, 345−353.

(18) Chung, L., Dinakarpandian, D., Yoshida, N., Lauer-Fields, J. L., Fields, G. B., Visse, R., and Nagase, H. (2004) Collagenase unwinds triple-helical collagen prior to peptide bond hydrolysis. *EMBO J. 23*, 3020−3030.

(19) Lauer-Fields, J. L., Chalmers, M. J., Busby, S. A., Minond, D., Fields, G. B., and Griffin, P. R. (2009) Identification of specific hemopexin-like domain residues that facilitate matrix metalloproteinase collagenolytic activity. *J. Biol. Chem. 284*, 24017−24024.

(20) Manka, S. W., Carafoli, F., Visse, R., Bihan, D., Raynal, N., Farndale, R. W., Murphy, G., Enghild, J. J., Hohenester, E., and Hideaki Nagase, H. (2012) Structural insights into triple-helical collagen cleavage by matrix metalloproteinase 1. *Proc. Natl. Acad. Sci. U.S.A. 109*, 12461−12466.

(21) Bertini, I., Lauer, J. L., Fragai, M., Luchinat, C., Fields, G. B., Melikian, M., and Toccafondi, M. (2012) Structural basis for matrix metalloproteinase 1-catalyzed collagenolysis. *J. Am. Chem. Soc. 134*, 2100−2110.

(22) Rosenblum, G., Van den Steen, P. E., Cohen, S. R., Grossmann, J. G., Jessica Frenkel, J., Sertchook, R., Slack, N., Strange, R. W., Opdenakker, G., and Sagi, I. (2007) Insights into the structure and domain flexibility of full-length pro-matrix metalloproteinase-9/gelatinase B. *Structure 15*, 1227−1236.

(23) Bertini, I., Calderone, V., Fragai, M., Jaiswal, R., Luchinat, C., Melikian, M., Mylonas, E., and Svergun, D. I. (2008) Evidence of reciprocal reorientation of the catalytic and hemopexin-like domains of full-length MMP-12. *J. Am. Chem. Soc. 130*, 7011−7021.

(24) Bertini, I., Fragai, M., Luchinat, C., Melikian, M., Mylonas, E., Sarti, N., and Svergun, D. I. (2009) Interdomain flexibility in full-length matrix metalloproteinase-1 (MMP-1). *J. Biol. Chem. 284*, 12821−12828.

(25) Rosenblum, G., Van den Steen, P. E., Cohen, S. R., Bitler, A., Brand, D. D., Opdenakker, G., and Sagi, I. (2010) Direct visualization of protease action on collagen triple helical structure. *PLoS One 5*, e11043.

(26) Cerofolini, L., Fields, G. B., Fragai, M., Geraldes, C. F. G. C., Luchinat, C., Parigi, G., Ravera, E., Svergun, D. I., and Teixeira, J. M. C. (2013) Examination of matrix metalloproteinase-1 in solution. *J. Biol. Chem. 288*, 30659−30671.

(27) Valdés, H., Díaz, N., Suárez, D., and Fernández-Recio, J. (2010) Interdomain conformations in the full-length MMP-2 enzyme explored by protein-protein docking calculations using pyDock. *J. Chem. Theory Comput. 6*, 2204−2213.

(28) Díaz, N., and Suárez, D. (2012) Alternative interdomain configurations of the full-length MMP-2 enzyme explored by molecular dynamics simulations. *J. Phys. Chem. B 116*, 2677−2686.

(29) Aimes, R. T., and Quigley, J. P. (1995) Matrix metalloproteinase-2 is an interstitial collagenase. *J. Biol. Chem. 270*, 5872−5876.

(30) Xu, X., Wang, Y., Lauer-Fields, J. L., Fields, G. B., and Steffensen, B. (2004) Contributions of the MMP-2 collagen binding domain to gelatin cleavage. Substrate binding via the collagen binding domain is required for hydrolysis of gelatin but not short peptides. *Matrix Biol. 23*, 171−181.

(31) Xu, X., Mikhailova, M., Ilangovan, U., Chen, Z., Yu, A., Pal, S., Hinck, A. P., and Steffensen, B. (2009) Nuclear magnetic resonance mapping and functional confirmation of the collagen binding sites of matrix metalloproteinase-2. *Biochemistry 48*, 5822−5831.

(32) Briknarová, K., Grishaev, A., Bányai, L., Tordai, H., Patthy, L., and Miguel Llinás, M. (1999) The second type II module from human

DOI: 10.1021/bi501014w
Biochemistry 2015, 54, 1243−1258

matrix metalloproteinase 2: Structure, function and dynamics. *Structure 7*, 1235−1245.
(33) Briknarová, K., Gehrmann, M., Bányai, L., Tordai, H., Patthy, L., and Llinás, M. (2001) Gelatin-binding region of human matrix metalloproteinase-2. *J. Biol. Chem. 276*, 27613−27621.
(34) Gehrmann, M. L., Douglas, J. T., Bányai, L., Tordai, H., Patthy, L., and Llinás, M. (2004) Modular autonomy, ligand specificity, and functional cooperativity of the three in-tandem fibronectin type II repeats from human matrix metalloproteinase 2. *J. Biol. Chem. 279*, 46921−46929.
(35) Díaz, N., Suárez, D., and Valdés, H. (2013) Unraveling the molecular structure of the catalytic domain of matrix metalloproteinase-2 in complex with a triple-helical peptide by means of molecular dynamics simulations. *Biochemistry 52*, 8556−8569.
(36) Lauer-Fields, J. L., Kele, P., Leblanc, R. M., Sui, G., Fields, G. B., and Nagase, H. (2003) Analysis of matrix metalloproteinase triple-helical peptidase activity with substrates incorporating fluorogenic L- or D-amino acids. *Anal. Biochem. 321*, 105−115.
(37) Morgunova, E., Tuuttila, A., Bergmann, U., Isupov, M., Lindqvist, Y., Schneider, G., and Tryggvason, K. (1999) Structure of human pro-matrix metalloproteinase-2: Activation mechanism revealed. *Science 284*, 1667−1670.
(38) Duan, Y., Wu, C., Chowdhury, S., Lee, M. C., Xiong, G., Zhang, W., Yang, R., Cieplak, P., Luo, R., Lee, T., Caldwell, J., Wang, J., and Kollman, P. (2003) A point-charge force field for molecular mechanics simulations of proteins based on condensed-phase quantum mechanical calculations. *J. Comput. Chem. 24*, 1999−2012.
(39) Jorgensen, W. L., Chandrasekhar, J., Madura, J. D., Impey, R. W., and Klein, M. L. (1983) Comparison of simple potential functions for simulating liquid water. *J. Chem. Phys. 79*, 926−935.
(40) Díaz, N., Suárez, D., and Valdés, H. (2008) From the X-ray compact structure to the elongated form of the full-length MMP-2 enzyme in solution: A molecular dynamics study. *J. Am. Chem. Soc. 130*, 14070−14071.
(41) Diaz, N., and Suarez, D. (2008) Molecular dynamics simulations of the active matrix metalloproteinase-2: Positioning of the N-terminal fragment and binding of a small peptide substrate. *Proteins 72*, 50−61.
(42) Bayly, C. I., Cieplak, P., Cornell, W., and Kollman, P. A. (1993) A well-behaved electrostatic potential based method using charge restraints for deriving atomic charges: The RESP model. *J. Phys. Chem. 97*, 10269−10280.
(43) Case, D. A., Darden, T. A., Cheatham, T. E., III, Simmerling, C. L., Wang, J., Duke, R. E., Luo, R., Crowley, M., Walker, R. C., Zhang, W., Merz, K. M., Wang, B., Hayik, S., Roitberg, A., Seabra, G., Kolossvary, K. F., Wong, K. F., Paesani, F., Vanicek, J., Wu, X., Brozell, S., Steinbrecher, T., Gohlke, H., Yang, L., Tan, C., Mongan, J., Hornak, V., Cui, G., Mathews, D. H., Seetin, M. G., Sagui, C., Babin, V., and Kollman, P. A. (2008) *AMBER 10*, University of California, San Francisco.
(44) Hooft, R. W. W., Vriend, G., Sander, C., and Abola, E. E. (1996) Errors in protein structures. *Nat. Rev. Cancer 381*, 272.
(45) Phillips, J. C., Braun, R., Wang, W., Gumbart, J., Tajkhorshid, E., Villa, E., Chipot, C., Skeel, R. D., Kalé, L., and Schulten, K. (2005) Scalable molecular dynamics with NAMD. *J. Comput. Chem. 26*, 1781−1802.
(46) Feig, M., Karanicolas, J., and Brooks, C. L. I. (2004) MMTSB Tool Set: Enhanced sampling and multiscale modeling methods for applications in structural biology. *J. Mol. Graphics Modell. 22*, 377−395.
(47) Case, D. A., Darden, T. A., Cheatham, T. E., III, Simmerling, C. L., Wang, J., Duke, R. E., Luo, R., Walker, R. C., Zhang, W., Merz, K. M., Roberts, B., Hayik, S., Roitberg, A., Seabra, G., Swails, J., Goetz, A. W., Kolossváry, I., Wong, K. F., Paesani, F., Vanicek, J., Wolf, R. M., Liu, J., Wu, X., Brozell, S. R., Steinbrecher, T., Gohlke, H., Cai, Q., Ye, X., Hsieh, M. J., Cui, G., Roe, D. R., Mathews, D. H., Seetin, M. G., Salomon-Ferrer, R., Sagui, C., Babin, V., Luchko, T., Gusarov, S., Kovalenko, A., and Kollman, P. A. (2012) *AMBER 12*, University of California, San Francisco.
(48) Frisch, M. J., Trucks, G. W., Schlegel, H. B., Scuseria, G. E., Robb, M. A., Cheeseman, J. R., Scalmani, G., Barone, V., Mennucci, B., Petersson, G. A., Nakatsuji, H., Caricato, M., Li, X., Hratchian, H. P., Izmaylov, A. F., Bloino, J., Zheng, G., Sonnenberg, J. L., Hada, M., Ehara, M., Toyota, K., Fukuda, R., Hasegawa, J., Ishida, M., Nakajima, T., Honda, Y., Kitao, O., Nakai, H., Vreven, T., Montgomery, J. A., Jr., Peralta, J. E., Ogliaro, F., Bearpark, M. J., Heyd, J., Brothers, E. N., Kudin, K. N., Staroverov, V. N., Kobayashi, R., Normand, J., Raghavachari, K., Rendell, A. P., Burant, J. C., Iyengar, S. S., Tomasi, J., Cossi, M., Rega, N., Millam, N. J., Klene, M., Knox, J. E., Cross, J. B., Bakken, V., Adamo, C., Jaramillo, J., Gomperts, R., Stratmann, R. E., Yazyev, O., Austin, A. J., Cammi, R., Pomelli, C., Ochterski, J. W., Martin, R. L., Morokuma, K., Zakrzewski, V. G., Voth, G. A., Salvador, P., Dannenberg, J. J., Dapprich, S., Daniels, A. D., Farkas, Ö., Foresman, J. B., Ortiz, J. V., Cioslowski, J., and Fox, D. J. (2009) *Gaussian 09*, revision B.01, Gaussian, Inc., Wallingford, CT.
(49) Becke, A. D. (1995) Exchange-Correlation Approximation in Density-Functional Theory. In *Modern Electronic Structure Theory Part II* (Yarkony, D. R., Ed.) World Scientific, Singapore.
(50) Rasolov, V. A., Pople, J. A., Patner, M. A., and Windus, T. L. (1998) 6-31G* basis set for atoms K through Zn. *J. Chem. Phys. 109*, 1223−1230.
(51) Baker, N. A., Sept, D., Joseph, S., Holst, M. J., and McCammon, J. A. (2001) Electrostatics of nanosystems: Application to microtubules and the ribosome. *Proc. Natl. Acad. Sci. U.S.A. 98*, 10037−10041.
(52) Pettersen, E. F., Goddard, T. D., Huang, C. C., Couch, G. S., Greenblatt, D. M., Meng, E. C., and Ferrin, T. E. (2004) UCSF Chimera: A visualization system for exploratory research and analysis. *J. Comput. Chem. 25*, 1605−1612.
(53) Kollman, P. A., Massova, I., Reyes, C., Kuhn, B., Huo, S., Chong, L., Lee, M., Lee, T., Duan, Y., Wang, W., Donini, O., Cieplak, P., Srinivasan, J., Case, D. A., and Cheatham, T. E. (2000) Calculating structures and free energies of complex molecules: Combining molecular mechanics and continuum models. *Acc. Chem. Res. 33*, 889−897.
(54) Gohlke, H., and Case, D. A. (2003) Converging free energy estimates: MM-PB(GB)SA studies on the protein−protein complex Ras−Raf. *J. Comput. Chem. 25*, 238−250.
(55) Swanson, J. M. J., Henchman, R. H., and McCammon, J. A. (2004) Revisiting free energy calculations: A theoretical connection to MM/PBSA and direct calculation of the association free energy. *Biophys. J. 86*, 67−74.
(56) Hansen, N., and van Gunsteren, W. F. (2014) Practical Aspects of Free-Energy Calculations: A Review. *J. Chem. Theory Comput. 10*, 2632−2647.
(57) Homeyer, N., and Gohlke, H. (2012) Free Energy Calculations by the Molecular Mechanics Poisson-Boltzmann Surface Area Method. *Mol. Inf. 31*, 114−122.
(58) Wright, D. W., Hall, B. A., Kenway, O. A., Jha, S., and Coveney, P. V. (2014) Computing Clinically Relevant Binding Free Energies of HIV-1 Protease Inhibitors. *J. Chem. Theory Comput. 10*, 1228−1241.
(59) Tamamis, P., and Floudas, C. A. (2013) Molecular recognition of CXCR4 by a dual tropic HIV-1 gp120 V3 loop. *Biophys. J. 105*, 1502−1514.
(60) Ylilauri, M., and Pentikäinen, O. T. (2013) MMGBSA as a Tool To Understand the Binding Affinities of Filamin−Peptide Interactions. *J. Chem. Inf. Model. 53*, 2626−2633.
(61) Palmer, D. S., Sørensen, J., Schiøtt, B., and Fedorov, M. V. (2013) Solvent Binding Analysis and Computational Alanine Scanning of the Bovine Chymosin−Bovine κ-Casein Complex Using Molecular Integral Equation Theory. *J. Chem. Theory Comput. 9*, 5706−5717.
(62) Osajima, T., Suzuki, M., Neya, S., and Hoshino, T. (2014) Computational and statistical study on the molecular interaction between antigen and antibody. *J. Mol. Graphics Modell. 53*, 128−139.
(63) Yang, Y., Liu, H., and Yao, X. (2012) Understanding the molecular basis of MK2-p38α signaling complex assembly: Insights into protein-protein interaction by molecular dynamics and free energy studies. *Mol. BioSyst. 8*, 2106−2118.

DOI: 10.1021/bi501014w
Biochemistry 2015, 54, 1243−1258

(64) Danielson, M. L., and Lill, M. A. (2012) Predicting flexible loop regions that interact with ligands: The challenge of accurate scoring. *Proteins: Struct., Funct., Bioinf. 80*, 246−260.
(65) Klett, J., Núñez-Salgado, A., Dos Santos, H. G., Cortés-Cabrera, Á., Perona, A., Gil-Redondo, R., Abia, D., Gago, F., and Morreale, A. (2012) MM-ISMSA: An Ultrafast and Accurate Scoring Function for Protein−Protein Docking. *J. Chem. Theory Comput. 8*, 3395−3408.
(66) Sharp, K., and Honig, B. (1991) Electrostatic Interactions in Macromolecules: Theory and Applications. *Annu. Rev. Biophys. Biophys. Chem. 19*, 301−332.
(67) Fennell, C. J., Kehoe, C., and Dill, K. A. (2010) Oil/Water Transfer Is Partly Driven by Molecular Shape, Not Just Size. *J. Am. Chem. Soc. 132*, 234−240.
(68) Suárez, D., and Díaz, N. (2015) Direct methods for computing single-molecule entropies from molecular simulations. *Wiley Interdiscip. Rev.: Comput. Mol. Sci. 5*, 1−26.
(69) Schlitter, J. (1993) Estimation of absolute and relative entropies of macromolecules using the covariance matrix. *Chem. Phys. Lett. 215*, 617−621.
(70) Schäfer, H., Mark, A. E., and van Gunsteren, W. F. (2000) Absolute entropies from molecular dynamics simulation trajectories. *J. Chem. Phys. 113*, 7809−7817.
(71) Schäfer, H., Daura, X., Mark, A. E., and van Gunsteren, W. F. (2001) Entropy Calculations on a Reversibly Folding Peptide: Changes in Solute Free Energy Cannot Explain Folding Behavior. *Proteins 43*, 45−56.
(72) Andricioaei, I., and Karplus, M. (2001) On the calculation of entropy from covariance matrices of the atomic fluctuations. *J. Chem. Phys. 115*, 6289−6292.
(73) Chang, C.-E., Chen, W., and Gilson, M. K. (2005) Evaluating the Accuracy of the Quasiharmonic Approximation. *J. Chem. Theory Comput. 1*, 1017−1028.
(74) Grossfield, A., and Zuckerman, D. M. (2009) Quantifying Uncertainty and Sampling Quality in Biomolecular Simulations. In *Annual Reports in Computational Chemistry* (Ralph, A. W., Ed.) Chapter 2, pp 23−48, Elsevier, Amsterdam.
(75) Díaz, N., and Suárez, D. (2008) Molecular dynamics simulations of the active matrix metalloproteinase-2: Positioning of the N-terminal fragment and binding of a small peptide substrate. *Proteins 72*, 50−61.
(76) Overall, C. M., and Butler, G. S. (2007) Protease yoga: Extreme flexibility of a matrix metalloproteinase. *Structure 15*, 1159−1161.
(77) Azhagiya Singam, E. R., Rajapandian, V., and Subramanian, V. (2014) Molecular dynamics simulation study on the interaction of collagen-like peptides with gelatinase-A (MMP-2). *Biopolymers 101*, 779−794.
(78) Murphy, G., Nguyen, Q., Cockett, M. I., Atkinson, S. J., Allan, J. A., Knight, C. G., Willenbrock, F., and Docherty, A. J. P. (1994) Assessment of the role of the fibronectin-like domain of gelatinase A by analysis of a deletion mutant. *J. Biol. Chem. 269*, 6632−6636.
(79) Steffensen, B., Wallon, U. M., and Overall, C. M. (1995) Extracellular matrix binding properties of recombinant fibronectin type II-like modules of human 72-kDa gelatinase/type IV collagenase. *J. Biol. Chem. 270*, 11555−11566.
(80) Nagase, H., and Fields, G. B. (1996) Human matrix metalloproteinase specificity studies using collagen sequence-based synthetic peptides. *Biopolymers 40*, 399−416.
(81) Lauer-Fields, J. L., Tuzinski, K. A., Shimokawa, K., Nagase, H., and Fields, G. B. (2000) Hydrolysis of triple-helical collagen peptide models by matrix metalloproteinases. *J. Biol. Chem. 275*, 13282−13290.
(82) Lauer-Fields, J. L., Broder, T., Sritharan, T., Chung, L., Nagase, H., and Fields, G. B. (2001) Kinetic analysis of matrix metalloproteinase activity using fluorogenic triple-helical substrates. *Biochemistry 40*, 5795−5803.
(83) Minond, D., Lauer-Fields, J. L., Nagase, H., and Fields, G. B. (2004) Matrix metalloproteinase triple-helical peptidase activities are differentially regulated by substrate stability. *Biochemistry 43*, 11474−11481.
(84) Minond, D., Lauer-Fields, J. L., Cudic, M., Overall, C. M., Pei, D., Brew, K., Visse, R., Nagase, H., and Fields, G. B. (2006) The roles of substrate thermal stability and P2 and P1′ subsite identity on matrix metalloproteinase triple-helical peptidase activity and collagen specificity. *J. Biol. Chem. 281*, 38302−38313.
(85) Bhaskaran, R., Palmier, M. O., Lauer-Fields, J. L., Fields, G. B., and Van Doren, S. R. (2008) MMP-12 catalytic domain recognizes triple helical peptide models of collagen V with exosites and high activity. *J. Biol. Chem. 283*, 21779−21788.

DOI: 10.1021/bi501014w
Biochemistry 2015, 54, 1243−1258